

SEAMLESS TRANSITION OF A MICROGRID BETWEEN
GRID-CONNECTED AND ISLANDED MODES

by

Julie B. Matarweh



A thesis

submitted in partial fulfillment

of the requirements for the degree of

Masters of Science in Electrical and Computer Engineering

Boise State University

August 2022

© 2022

Julie B. Matarweh

ALL RIGHTS RESERVED

BOISE STATE UNIVERSITY GRADUATE COLLEGE

DEFENSE COMMITTEE AND FINAL READING APPROVALS

of the thesis submitted by

Julie B. Matarweh

Thesis Title: Seamless Transition of a Microgrid Between Grid-Connected and Is-
landed Modes

Date of Final Oral Examination: 27 April 2022

The following individuals read and discussed the thesis submitted by student Julie B. Matarweh, and they evaluated the student's presentation and response to questions during the final oral examination. They found that the student passed the final oral examination.

Said Ahmed-Zaid, Ph.D. Chair, Supervisory Committee

Thaddeus Welch, Ph.D. Member, Supervisory Committee

Andres Valdepena Delgado, Ph.D. Member, Supervisory Committee

The final reading approval of the thesis was granted by Said Ahmed-Zaid, Ph.D., Chair of the Supervisory Committee. The thesis was approved by the Graduate College.

ACKNOWLEDGMENT

I would like to express my special thanks of gratitude to my advisor Prof. Said Ahmed-Zaid for guiding me through my thesis as well as to Prof. Thad Welch for providing me with a full year scholarship. I would like to also thank Dr. Andrés Valdepeña Delgado for giving me great ideas and guiding me through my research.

I would like to express my gratitude to my beloved husband and family who encouraged me to achieve this goal. Without their tremendous help and understanding, it would have been impossible for me to complete my studies.

ABSTRACT

This thesis focuses on improving the behavior of inverters during transition periods from islanded mode to grid-connected mode (GC) and vice-versa. A systematic approach is presented to add smart features to inverters to enhance their capability to cope with sudden changes in the power system.

The importance of microgrids lies in their ability to provide a stable and reliable source of power for critical loads in the presence of faults. For this purpose, a design is proposed consisting of a distributed energy resource (DER), battery energy storage system (BESS) and a load connected through a bypass switch with the main utility distribution substation. The BESS is connected to the AC distribution feeder through a smart inverter that is controlled in both modes of operations. The system was tested using MATLAB/Simulink models and the results show proof of the seamless transition between the two modes of operation. The cost of building the software system was unnoticeable due to the availability of a MATLAB license but the real cost of the hardware needed to build the system will be moderate though the importance will be significant.

Keywords: Grid-Connected Mode, Islanded Mode, Microgrid, Smart Inverter, PLL

TABLE OF CONTENTS

ACKNOWLEDGMENT	iv
ABSTRACT	v
LIST OF FIGURES	ix
LIST OF TABLES	xi
1 INTRODUCTION	1
1.1 Scope of the Work	2
1.2 Background and Literature Review	2
1.3 Outline of Thesis	3
2 AC MICROGRIDS AND SMART INVERTERS	5
2.1 Introduction	5
2.2 Microgrids	6
2.2.1 Grid-Connected Mode (GC)	7
2.2.2 Islanded Mode	7
2.3 Smart Inverters	7
2.3.1 Types of Smart Inverters	8
2.3.2 Functionalities of Smart Inverters	9

2.4	IEEE Standard 1547-2018	10
2.4.1	Voltage Mandatory Tripping and Ride Through	11
2.4.2	Frequency Mandatory Tripping and Ride Through	12
2.4.3	Unintentional Islanding	12
2.4.4	Intentional Islanding	13
2.5	Microgrid Control Hierarchy	14
2.5.1	Primary Control	14
2.5.2	Secondary Control	14
2.5.3	Tertiary Control	15
3	MODELING OF MICROGRIDS	16
3.1	Introduction	16
3.2	Basic Components of Microgrids	17
3.2.1	Photovoltaic (PV) System	17
3.2.2	Battery Energy Storage System	18
3.2.3	LC Filter	20
3.2.4	Load model	24
3.3	Pulse Width Modulation	24
3.4	Phase-Locked Loop	25
3.5	dq0-Frame Representation	27
4	DESIGN AND CONTROL STRATEGY	30
4.1	Introduction	30
4.2	Control Schemes	31
4.2.1	Grid-Connected Mode Control Scheme	31

4.2.2	Islanded Mode Control Scheme	39
4.2.3	Transition Mode Control Scheme	42
4.3	Fault Detection	43
5	RESULTS	46
5.1	Introduction	46
5.2	Design Parameters	47
5.2.1	Grid Parameters	47
5.2.2	Inverter Parameters	47
5.2.3	LC filter Parameters	48
5.3	Grid-Connected Simulation	50
5.4	Islanded Simulation	54
5.5	Self-Detection Simulation	58
6	CONCLUSIONS AND FUTURE WORK	60
6.1	Conclusions	60
6.2	Future Work	61
	REFERENCES	62
	APPENDICES	67
A	WECC DYNAMIC MODULES	68
B	PASSIVE ELEMENTS IN DQ0-TRANSFORMATION	72

LIST OF FIGURES

2.1	Microgrid	6
3.1	Three Phase Source in Simulink Model	17
3.2	Maximum Power Point Tracker	18
3.3	Comparison of Battery Recycling: Lead-Acid Vs. Lithium-Ion	20
3.4	Grid-Connected Three Phase Diagram	21
3.5	Grid-Connected Single Phase Diagram	21
3.6	Grid-Connected Three Phase Diagram	25
3.7	Block Diagram of a Phase-Locked Loop (PLL)	26
3.8	alpha-beta to dq-transformation	27
4.1	Grid-Connected Equivalent	32
4.2	Grid-Connected Control	35
4.3	Control Block Diagram of a current controlled VSC system	37
4.4	Islanded Mode Equivalent	40
4.5	Islanded Mode schematic	40
4.6	Islanded Mode Cascaded Solution	42
4.7	Seamless transition Solution	43
4.8	Fault Detection	44
4.9	Flowchart of Fault Detection Criteria	45

5.1	Grid-Connected Control	50
5.2	Grid Voltage (V_s) and Current (I_s) in Grid-Connected mode	52
5.3	Grid Frequency in Grid-Connected mode	52
5.4	Inverter Terminal Voltage (V_T) and Current (I_T) in Grid-Connected Mode	53
5.5	Load Voltage (V_L) and Current (I_L) in Grid-Connected Mode	53
5.6	Islanded Mode schematic	55
5.7	Grid Voltage (V_s) and Current (I_s) in Islanded mode	56
5.8	Grid Frequency in Islanded mode	56
5.9	Inverter Terminal Voltage (V_T) and Current (I_T) in Islanded Mode	57
5.10	Load Voltage (V_L) and Current (I_L) in Islanded Mode	57
5.11	Switching Scheme	58
A.1	Block Diagram Representation of the BESS Model	69
A.2	Block Diagram of Renewable Energy Generator/Converter Module	70
A.3	Block Diagram of Renewable Energy Control Module	71

LIST OF TABLES

2.1	DER response (shall trip) to abnormal voltages for DER of abnormal operating performance category I	11
2.2	DER response (shall trip) to abnormal voltages for DER of abnormal operating performance category II	12
2.3	DER response (shall trip) to abnormal voltages for DER of abnormal operating performance category III	12
2.4	Voltage and Frequency Acceptable Range for Category I, II, and III DERs	13
5.1	Grid Parameters	47
5.2	IGBT of VSC Parameters	48
5.3	The LCL Filter Parameters	48
5.4	Design Acronyms	49

CHAPTER 1:

INTRODUCTION

There has been an overwhelming growth of the global population in the last few decades, with an increase of around 700 million people from 2011 to 2019 [1]. This population increase has led to a huge rise in the demand for electrical energy. Electricity is generated in power plants and transmitted through long transmission lines and cables to cities, and distributed among the neighborhoods through substations. This source of energy is divided into non-renewable energy resources such as fossil fuel and nuclear power plants or renewable energy resources such as solar energy, wind energy and hydro energy.

However, the greenhouse emissions from burning fossil fuels are causing environmental instability and increasing pollution. Therefore, the importance of renewable energy has increased in the last two decades, due to its high capability of providing a never-ending source of energy, without leaving any harmful waste to the environment. However, the unpredictable, unreliable nature of renewable energy makes it hard to control. So, the need of having a rigid and stable control system in order to fulfill the energy need is of the highest priority. On the other hand, many laws and regulations are being implemented around the world to mitigate the effect of global warming, thus, meeting the global environmental standards is a top concern of many countries.

1.1 Scope of the Work

The main objective of this research is to discuss the control behavior of smart inverters and voltage source converters (VSC) in microgrids (MG) through two different modes of operations: Grid-connected (GC) Mode and Islanded Mode. It also explains the operation of distributed energy resources (DERs), such as battery energy storage systems (BESS) and photovoltaic (PV) in microgrids. This work focuses mainly on finding a solution for reducing voltage and current transients during transition periods between islanded mode and grid-connected mode. The proposed solution in this thesis is a design of a control methodology that maintains the voltage and frequency of the system within the IEEE-1547 standard limits during the transition period between grid-forming and grid-following behavior. The smooth transition between the two states is important for the power quality of the power system, as well as for the protection of the load equipment.

1.2 Background and Literature Review

During catastrophic weather events, microgrids provide little to no downtime of electricity due to their high reliability and ability to isolate quickly from the main grid. The importance of microgrids is essential for utility grid resilience and the improvement of the security of power supply to critical loads [2], [3]. Recent studies have implemented extended research on the improvement of BESS in microgrids [4], [5]. This includes a battery management system (BMS) compatible with a PV system that is regulating the state of charge of the batteries . In reference [6], a droop control method was proposed to implement a seamless transfer strategy for the DERs, where a bypass switch was used to transfer between both modes of operation after synchro-

nization, in order to avoid a frequency and phase oscillations. In reference [7], an AC microgrid was controlled through a distributed hierarchical three-level control system, which is basically a droop control, distributed follower control and a supervisory control system. In reference [8], the author proposed two parallel inverters working together to achieve the best power sharing techniques between the PV and the wind system, with one inverter depending on a voltage-controlled and current-controlled behavior, and the other inverter just settling for power control loop.

1.3 Outline of Thesis

The structure of this thesis will be as follows:

- Chapter 1 introduces the problem and the scope of the work. It also contains some background research implemented on this topic.
- Chapter 2 provides more detailed definitions for the modes of operation of a VSC in a microgrid. It includes some of the smart features of smart inverters and the techniques that should be implemented to get the best results. The IEEE 1547-2018 standards are summarized and included in this chapter as well.
- Chapter 3 discusses the basic components of microgrids and many techniques used in the simulation model; such as PWM, PLL and dq-frame representation.
- Chapter 4 defines the control strategies implemented, with full details on the calculations used to implement the models. The models discussed are the grid-connected mode, the islanded mode and the transition mode.
- Chapter 5 discusses the results of the Simulink simulations with brief calculations on the design parameters.

- Chapter 6 provides a conclusion and future work plans.

CHAPTER 2:

AC MICROGRIDS AND SMART INVERTERS

2.1 Introduction

Based on U.S. Energy Information Administration (EIA) data, the electricity infrastructure in the United States is providing 1 million megawatts of generating capacity, which makes it an engineering brilliance. However, with the high penetration of renewable energy resources and the continuing increase in demand for electricity, the electric grid is experiencing a reduction in the reliability and security of the power system. Therefore, microgrids (MG) have been proposed to maintain a high resilient compatibility between the distributed generators (DG) with the main utility grid. A microgrid is a small network of electricity users and electric sources that are connected to each other. It usually operates connected to the main grid, but is able to disconnect itself during faults caused by natural disasters or an unpredictable loss of power [9]. Figure 2.1 shows a model of a microgrid consisting of several DERs connected with each other through a controller. This controller is able to communicate and control the main bypass switch that acts as an interface between the grid and microgrid.

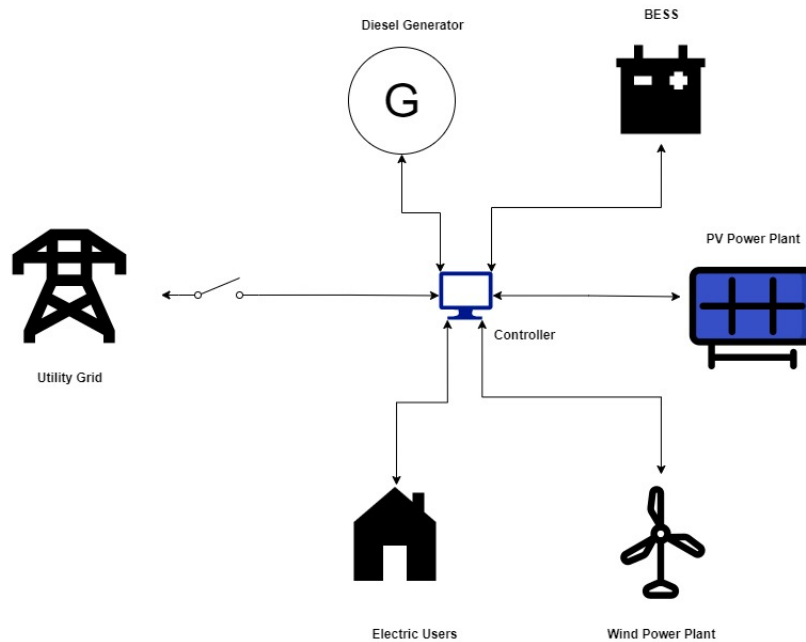


Figure 2.1: Microgrid

2.2 Microgrids

An MG makes it easier to cope with the high diffusion of DGs, and it allows users to take an active part in the energy generation process by enabling them to choose their energy consumption behavior by providing them with smart metering units and smart energy generation applications. On the other hand, MGs are considered a huge support to the utility grid due their capability of providing critical loads with an uninterrupted supply of energy during faults. Most MGs are connected to the main grid through a bypass switch and are able to export and import energy to the main grid through power converters such as smart inverters. They operate in two modes of operations: grid-connected mode and islanded mode, which will be explained briefly in the following sections.

2.2.1 Grid-Connected Mode (GC)

During normal operations, both the voltage and the frequency of the system are regulated by the utility grid. Accordingly, the microgrid will be exchanging real and reactive power between the DGs and the grid to supply the loads [10]. In this mode of operation, all the power converters in the microgrid are acting in the grid-following mode (PQ-control mode), which means they follow the utility voltage and frequency; thus, the smart inverters will be operating as a current source to enable the exchange of power.

2.2.2 Islanded Mode

During faults in the main grid or when maintenance is needed in any part of the power system, the MG is isolated manually or automatically by opening the bypass switch. Consequently, the smart inverters will be responsible for regulating the voltage and the frequency of the microgrid. Thus, it will be running in the grid-forming mode (VF-control mode) of operation [10]. In this state, the VSC will be acting as a voltage source to the islanded grid. On the other hand, achieving power sharing throughout the system is critical and needs to be maintained during this mode.

2.3 Smart Inverters

Smart inverters are considered one of the fundamental components of MGs. They act as the communication interface between the distributed generators and other components. Smart inverters are capable of controlling the behavior of microgrids during different modes of operation as they are the brain of the microgrid. Their smart features enable them to interact with the grid to provide additional support to the MG during faulty times. As per the WECC (Western Electricity Coordinating Council)

Battery Storage Guideline; ‘the power converter in BESS are voltage source converters and allow full four quadrant control on the active and reactive current output independently within the current rating limits of the power electronics (IGBTs). Four quadrant control means the real current flow directions can represent either charging or discharging states, while the reactive current flows can represent either supplying or absorbing reactive power simultaneously and independently. This type of power converter is normally referred as a voltage source converter (VSC).’ Some microgrids contain a number of converters that are divided into two categories based on which follows orders (followers) and which gives them (Master). Also, smart inverters can be single phase or three phases based on the needed load type. The following sections will explain each type of inverter and their functionalities.

2.3.1 Types of Smart Inverters

There are two types of control techniques that are implemented in the microgrid industry; the centralized control technique and the decentralized control technique [11]. The master-follower technique and the distributed control technique are the most important applications of the centralized control scheme and they will be explained next.

Master-Follower Technique

As mentioned before, the inverter should act as a voltage source in order to form a base voltage for the whole microgrid. This operation is called a grid-forming process and it is applied by the master inverter. In the master-follower control technique, microgrids have their main DER (mainly the energy storage system (ESS)) inverter to be the master inverter that is required to form the voltage and the frequency of

the grid, while the other DERs have following inverters (current-forming) that will always follow the master inverter voltage and frequency [11].

One drawback of this technique is that one master inverter will not be sufficient to form the voltage and frequency in the case of many dynamic loads. Also, communication links should connect the inverter with a reference signal that enables the sharing of the phase and frequency of the signal in order to provide quick synchronization with the grid. Furthermore, in case of misoperation or maintenance of the master inverter, another follower inverter should convert to a master inverter to insure continuity of service. Nevertheless, the power sharing capability of this technique is outstanding.

Distributed Control Technique

The main idea of this technique is that all of the DER inverters are acting as a master inverter (grid-forming), which means each inverter regulates the voltage and the frequency and synchronizes them with the grid. This control scheme is slightly different because it depends on the average current of each inverter, which is the current at the point of common coupling divided by the number of inverters in the microgrid [11],[12].

2.3.2 Functionalities of Smart Inverters

The following are some of the advanced features of smart inverters;

Autonomous Capabilities “Ride Through”

Ride through is the capability of a smart inverter to continue working through faulty times, such as frequency and voltage disturbances in the grid. Nowadays, with the massive development of protection systems, smart inverters have the ability to trip

offline quickly to prevent any critical damage to the equipment. On the other hand, they have little to slow capability to go back online when things go back to normal. With the high penetration of renewable energy resources connected to the grid, this might cause a high amount of renewable power to be lost due to frequency and voltage disruptions. Some countries and states such as California and Hawaii, that have many DERs have developed their own ride-through standards to overcome this problem (e.g, California Rule 21 and Hawaii Rule 14).

Autonomous voltage and active/reactive power control capabilities

The power production of DERs vary over time, so the inverters introduce voltage fluctuations in the grid. One of the most fundamental features of smart inverters is their capacity to diminish impacts on the grid by changing their mode of operation through modulating real and reactive power.

Communication capabilities

One of the features that is obligatory by the IEEE-1547-2018 standard is the ability of the utilities to control and communicate with smart inverters easily. This will improve the microgrid management and controlling features, which in turn minimizes the damages to the grid during misoperations.

2.4 IEEE Standard 1547-2018

IEEE 1547 (Standard for Interconnecting Distributed Resources with Electric power Systems) is a standard that is set to provide criteria and a number of requirements for the interconnection of distributed generators on the grid [13]. In this project, the smart inverter settings and control systems should abide by the IEEE 1547 standards

relating to the voltage and frequency of the system.

2.4.1 Voltage Mandatory Tripping and Ride Through

The voltage mandatory tripping regulation has a main intention of providing safety for maintenance workers and the public. Furthermore, if the voltage is outside a certain acceptable boundary, it might cause damage to the power system equipment and the distributed generators. Thus, the Institute of Electrical and Electronics Engineers (IEEE) had to implement the regulations for the adequate voltage thresholds that will help minimize the adverse outcome if any disturbances or abnormal events happen in the future. The tripping should happen if the faulted value continues to occur after a specific period of clearing time. It is important to mention that the voltage and time set points should be adjustable in the field or remotely.

Tables 2.1, 2.2 and 2.3 summarize the DER response to abnormal voltages for DER of abnormal operating performances provided by the IEEE 1547-2018 [13] of category I (essential bulk power systems reliability/stability), category II (all bulk power systems reliability/stability) and category III (both bulk power system and distribution system reliability/stability), respectively. Two overvoltage trip functions have limitations (OV1, OV2), Also, two undervoltage trip functions have limitations (UV1, UV2).

Table 2.1: DER response (shall trip) to abnormal voltages for DER of abnormal operating performance category I

Shall trip function	OV2	OV1	UV1	UV2
voltage (pu of nominal voltage)	1.2	1.10	0.7	0.45
Clearing Time (s)	0.16	2	2	0.16

Table 2.2: DER response (shall trip) to abnormal voltages for DER of abnormal operating performance category II

Shall trip function	OV2	OV1	UV1	UV2
voltage (pu of nominal voltage)	1.2	1.10	0.7	0.45
Clearing Time (s)	0.16	2	10	0.16

Table 2.3: DER response (shall trip) to abnormal voltages for DER of abnormal operating performance category III

Shall trip function	OV2	OV1	UV1	UV2
voltage (pu of nominal voltage)	1.2	1.10	0.88	0.5
Clearing Time (s)	0.16	13	12	0.16

2.4.2 Frequency Mandatory Tripping and Ride Through

The frequency mandatory tripping also has tripping and ride-through requirements that must be applied to ensure the support of the DER systems to the bulk power system during an abnormal contingency that might occur in the system, in addition to the ability of the DER to ride through frequency disturbance events in the power system.

2.4.3 Unintentional Islanding

Unintentional islanding occurs when a part of a grid is being energized by one or more DER's while it is electrically isolated from the grid. The part that is being isolated is called an island and the DER is required to “detect the island, cease to energize the area EPS, and trip within two seconds of the formation of an island” [13]. This operation is considered a concern for many researches due to the fact that the utility loses control of the system's voltage and frequency. This might cause severe damage

Table 2.4: Voltage and Frequency Acceptable Range for Category I, II, and III DERs

Service Criteria	Objective
Applicable Voltage within Range	$0.88 \text{ pu} < V \text{ (pu)} < 1.1 \text{ pu}$
Applicable Frequency within Range	$58.5 < F \text{ (Hz)} < 60.6$

to the equipment connected to the grid [14]. In this thesis, unintentional islanding will not be further investigated.

2.4.4 Intentional Islanding

Intentional islanding can be divided into scheduled and unscheduled islanding. In this thesis, intentional islanding is taken into consideration [15].

Scheduled Intentional Islanding

Scheduled intentional islanding can be planned ahead to isolate the island from the main grid. As mentioned before, some critical loads need to have an uninterrupted supply of power when the main grid is going through some enhanced reliability, economic dispatch, maintenance or foreseen extreme weather. The microgrid can be manually isolated by opening the main bypass switch connecting the main utility grid to the island [16].

Unscheduled Intentional Islanding

Unscheduled intentional islanding is the process of autonomously isolating the microgrid from the grid due to disruptions and faults on the main grid. The smart DER should be able to detect and give commands to isolate automatically from the grid to provide an uninterrupted supply of power to the critical load while the main grid

is undergoing some failures.

2.5 Microgrid Control Hierarchy

The control hierarchy in microgrids is essential in the management of the system. There is no general structure, since each microgrid has their own configuration based on the available infrastructure, but it is mostly identified by three levels of controls; where each level has their own communications regulations and certain time requirements to enable the continuity of service for critical loads. These controls are divided as follows.

2.5.1 Primary Control

The primary control in the microgrid control hierarchy is considered the most essential of all. It has the shortest time response but needs a high capability communication link with the main grid. In this thesis, Islanding detection is considered in the primary control of the hierarchy due to its quick response to any voltage and frequency fluctuations in the grid [17], [18]. Moreover, the controller of the smart inverter receives instantaneous set points of the grid voltage and frequency in order to make a decision whether to go to islanded mode or not.

2.5.2 Secondary Control

Secondary control ensures that the values of the microgrid are within the required limits. It usually involves providing current and voltage control loops to establish stable output power from the smart inverters in islanding mode. Moreover, it ensures a seamless transition to keep the synchronization process with minimal fluctuations and transients [19]. This process prevents any damage to the equipment connected to the grid by providing smooth and clean power.

2.5.3 Tertiary Control

In this level of control, the microgrid should manage the power flow between the different DERs with the grid. In some research, they provide an economic dispatch study in this level to ensure the cheapest and most convenient DER to be supplying the most power at different times of the day. In this thesis, tertiary control will not be further investigated.

CHAPTER 3:

MODELING OF MICROGRIDS

3.1 Introduction

Modelling the different components of the microgrid can be tricky, especially with the restricted regulations of different electricity standards and councils, such as the IEEE guidelines and the WECC (Western Electricity Coordinating Council). In recent years, the WECC has worked with different utilities and organizations to develop different ‘generic’ models for renewable components of microgrids, such as wind and Photovoltaic (PV) systems. These models are computer-based simulation models that are open for public use in different software, such as the GE/PSLF transmission planning software. The WECC used the same concept in developing a model for BESS by using a combination of some renewable modules that have already been implemented, such as the converter model. The REGC_B Module is used to represent the converter interface with the grid, while the REEC_D module which represents the Battery System is augmented from the REEC_A that represents a wind turbine generator or a PV system. The main highlights between the two modules is that the REEC_D accounts for the state of charge (SOC), which will be explained briefly in Section 3.2.2. The REPC is used to represent the plant controller. More information on this model can be found in Appendix A.

In the previous chapter, we introduced the various types of control hierarchies and a background view of the IEEE regulations with regards to acceptable voltage and frequency range. The different parts of the power system used in this thesis are discussed next. In MATLAB/Simulink, it is important to mention that the utility grid power system can be modeled with a three phase source, as shown in Figure 3.1. It is assumed that this source represents the low side of a distribution power system substation. In the following sections, the basic components of a microgrid will be briefly explained and introduced.

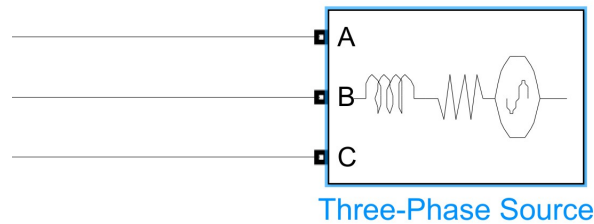


Figure 3.1: Three Phase Source in Simulink Model

3.2 Basic Components of Microgrids

3.2.1 Photovoltaic (PV) System

A PV system is a renewable energy resource that converts solar photons into DC electric energy. Each PV cell is manufactured using different materials, such as silicon or cadmium telluride. However, a number of PV cells can be connected with each other through series and parallel connections to form what is called a PV panel. The number of series and parallel PV cells is determined by the output voltage and current needed from the PV panel. A PV string is multiple PV panels connected with each

other, and a PV array is many PV strings connected with each other with a PV inverter [20]. Generally, a PV system is connected to a DC/AC inverter through a Maximum Power Point Tracker (MPPT). The MPPT tracker allows the system to choose the optimum voltage to produce the maximum output power for the PV system, as shown in Figure 3.2. The MPPT tracker can use different schemes and models such as the Perturb and Observe (PO) method, fuzzy logic Scheme [21] [22], Hill Climbing (HC) scheme [23], and Incremental Conductance (IC) scheme. Usually, a smart inverter includes a MPPT internally to make it compatible with sudden weather changes and load disturbances. In this thesis, a DC source will be used to model a PV system for easier implementation.

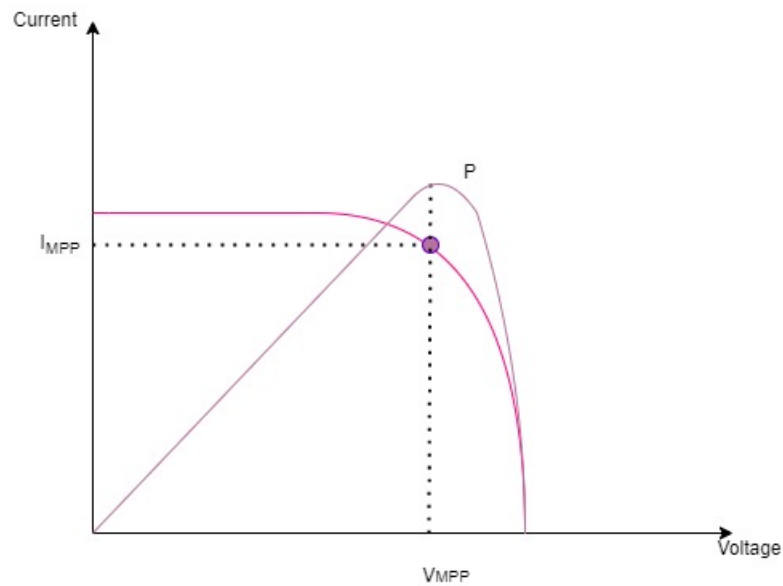


Figure 3.2: Maximum Power Point Tracker

3.2.2 Battery Energy Storage System

A battery is an electrochemical device that charges energy and stores it. The source of energy might be from the grid or from another renewable energy resource. These

storage systems discharge their energy through wires when power sharing services are needed in the grid, or when the the microgrid is in islanded mode. These devices are a relatively new technology that enables the microgrid to store energy for later use. Lithium-Ion batteries are the most commonly used in this industry, due to their high power density [24], life cycle and high recycling usage. They are also known for their high percentage of usable energy, that can extend up to 80% in comparison with 50% for lead-acid batteries. Lead acid batteries are considered unreliable and takes up considerable floor space, Also, lead acid batteries are heavier in weight, which might be expensive due to the need of reinforcing floors to handle the extra weight. Furthermore, lead acid batteries contain large amounts of toxic materials, such as lead and sulfuric acid, that are harmful for the environment [25]. Figure 3.3 from the EPRI Journal shows a comparison of battery recycling between lead-acid and lithium-ion batteries [26]. The figure is divided to 4 different categories of the recycling levels, it shows how the lithium-ion batteries high valued metals can be captured and used in other industries. Many battery cells can be connected in series and parallel to compose a battery module which is packed in a cell. The battery string is many modules connected with each other in a series connected with the battery monitoring circuit, communication interfaces and heat management devices.

Modelling battery systems with an optimized battery management system can be tricky due to many factors that are inherently associated with the decision making process [27]. These factors include the state of charge of the battery, the surrounding temperatures, and many more. In this thesis, a DC source is used to model a lithium-Ion based battery system to make the simulation faster and less complex.

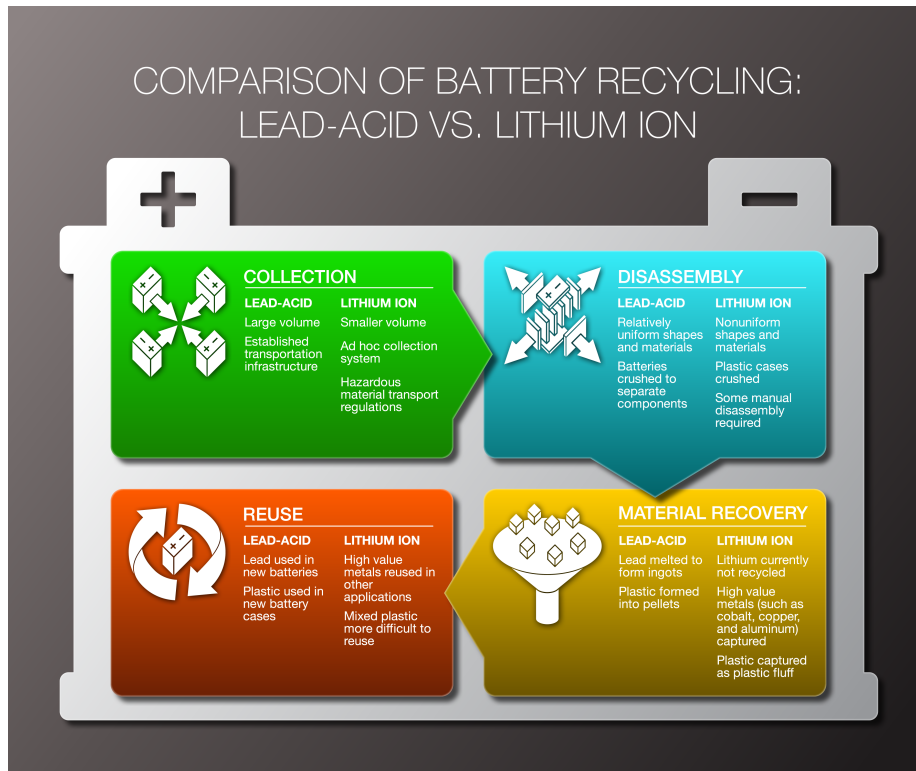


Figure 3.3: Comparison of Battery Recycling: Lead-Acid Vs. Lithium-Ion

3.2.3 LC Filter

In this thesis, a two-level three phase inverter that contains six transistors that quickly alternate through a switching scheme is modelled. The output of the inverter contains many harmonics and noise that needs to be filtered out. An LC or LCL filter is required to minimize the voltage and current harmonics that are caused by the switching devices in order to maximize the power quality. The filter contains passive elements of inductors in series and a shunted capacitor. In MATLAB/Simulink, the LC filter is modelled based on the following design procedure. First, an LCL filter calculation design method will be proposed and then an LC filter will be implemented. The 3-phase grid connected system with an LCL filter can be represented, as shown

in Figure 3.4.

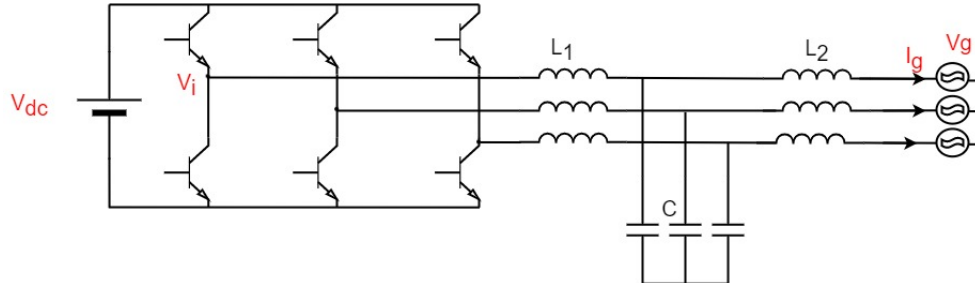


Figure 3.4: Grid-Connected Three Phase Diagram

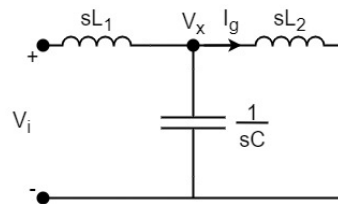


Figure 3.5: Grid-Connected Single Phase Diagram

In order to get the transfer function between the output current I_g with respect to the input voltage, a superposition methodology is applied to short circuit the grid voltage in a single-phase representation, as seen in Figure 3.5.

Then a KCL node equation is applied to get Equation (3.1)

$$\frac{V_i - V_x}{sL_1} = I_g + \frac{V_x}{\frac{1}{sC}}, \quad (3.1)$$

and Ohm's law is applied to get Equation (3.2),

$$V_x = I_g sL_2, \quad (3.2)$$

Solving those equations together, we get:

$$\frac{I_g}{V_i} = \frac{1}{s^3 L_1 L_2 C + s(L_1 + L_2)}, \quad (3.3)$$

Let us assume:

$$L_1 + L_2 = L, \quad (3.4)$$

and

$$L_p = \frac{L_1 L_2}{L_1 + L_2}, \quad (3.5)$$

A simplified transfer function can be obtained as follows:

$$\frac{I_g}{V_i} = \frac{1}{sL(1 + s^2 C L_p)}, \quad (3.6)$$

From the above equation, it can be shown that the resonance frequency is:

$$\omega_{res} = \frac{1}{\sqrt{C L_p}}, \quad (3.7)$$

The following steps show a detailed design criteria for choosing the inductor and capacitor values:

Step 1: The switching frequency F_{sw} is chosen to be 10 kHz.

Step 2: The resonance frequency F_{res} is chosen to be far away from the switching

frequency and the fundamental frequency. A thumb rule is $F_{res} = \frac{F_{sw}}{10} = 1000$ Hz.

Step 3: In order to find the value of the capacitance, the following equation can be used:

$$Q = \frac{V^2}{X_c}, \quad (3.8)$$

, And knowing as a rule of thumb, the reactive power absorbed by the capacitor is 0.05 of the rated apparent power (S) of the system [28], we get,

$$C = \frac{0.05S}{V^2 \times 2 \times \pi \times f}, \quad (3.9)$$

Step 4: In order to find the value of the inductor, two methods can be applied, The first one depends on the resonant and switching frequency and can be summarized as follows. Based on Equations (3.6) and (3.7), we can derive the following equation:

$$L = \frac{1}{\omega_{sw} \times \frac{I_{g(sw)}}{V_{i(sw)}} \times \left(1 - \frac{\omega_{sw}^2}{\omega_{res}^2}\right)}, \quad (3.10)$$

From IEEE 519-2014 standard, the $I_{g(sw)}$ is equal to 0.3 of the I_g and based on a triangular sine PWM Scheme, the minimum value of V_i equals 0.9 of V_g .

The other method is to design the inductor is based on the voltage drop across it, and a voltage drop has a maximum applicable value of 0.2 of the grid voltage, as seen in the following equation,

$$L = \frac{0.2V_g}{2\pi fI}, \quad (3.11)$$

To sum up, the LC filter used in the design will be based on Equations (3.11) and (3.9), and they will be placed at the output of the inverter (VSC) in order to filter out the harmonics.

3.2.4 Load model

Load models can be divided into static or dynamic loads. Static loads are constant loads that consume the same amount of power at any instance of time. On the other hand, dynamic loads are time variant loads which change the amount of power consumed. In this thesis, only static resistive loads will be modelled due to the high complexity of control models of dynamic loads.

3.3 Pulse Width Modulation

Pulse Width Modulation (PWM) is a technique that converts a DC signal to an AC signal by controlling the behavior of a number of switching devices by turning them on and off in a specific alternating scheme [29]. In general, PWM is used in inverters to generate a desired output by comparing a reference signal called the modulation signal (M_d) with a high frequency periodic triangular waveform called the carrier signal. If the modulating signal is smaller than the reference signal at one instant of time, then a switch turns on and stays on until the modulating signal becomes larger than the reference signal again, and then the switch turns off, as shown in Figure 3.6.

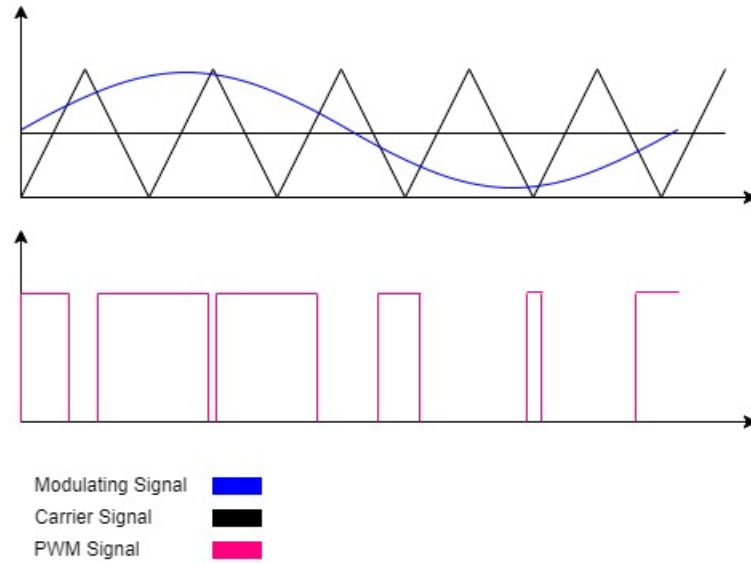


Figure 3.6: Grid-Connected Three Phase Diagram

3.4 Phase-Locked Loop

A phase-locked loop (PLL) is a control scheme for the MG that is used to generate an output signal (inverter output power) whose phase is related to the phase of the input signal (grid). In other words, a PLL is used to synchronize the inverter output current with the grid voltage and, in our model, a PLL is used to lock the phase and frequency of the inverter to the grid during the synchronization process. In the case of sending active power to the grid, the inverter should generate a current which is in phase with the grid voltage. Then, we should use a PLL to generate a reference signal with a magnitude between 1 and -1 which is in phase with the grid voltage. On the other hand, sending reactive power will require the inverter to generate current which is out of phase by 90 degrees with the grid voltage. A PLL may have two different control schemes. A simple method will transform the input signal from three-phase to alpha-beta coordinates and obtain an angle using the following equation:

$$\theta = \cos^{-1} \left(\frac{V_\alpha}{\sqrt{V_\alpha^2 + V_\beta^2}} \right), \quad (3.12)$$

However, this method is considered an algebraic method with an open loop system, so it cannot withstand any disruptions in the signal such as harmonics, noise or spikes. The other PLL method, which is considered the most appropriate in our case, is a closed loop system with a feedback scheme that keeps our system stable under abrupt situations, and it is explained in Figure 3.7. First, we need to transform the signal into the dq frame, where ωt is the angle between V_α and the d-axis. Then, we will consider $V_q=0$, so now V_d will be aligned with the V_β (grid) axis, as seen in Figure 3.8. The new ωt will be used to generate the active and reactive power reference signals. A PI controller is used to keep the q-value zero, so the voltage can be represented by only a direct-axis component.

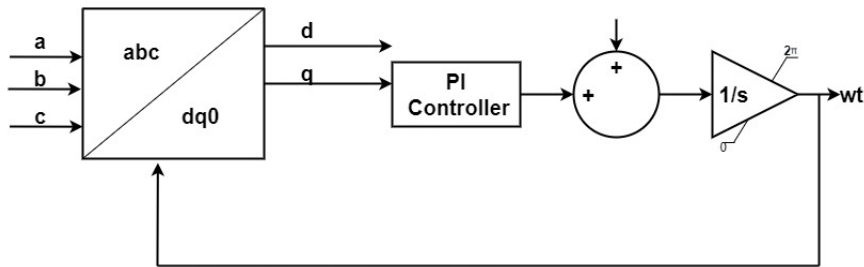


Figure 3.7: Block Diagram of a Phase-Locked Loop (PLL)

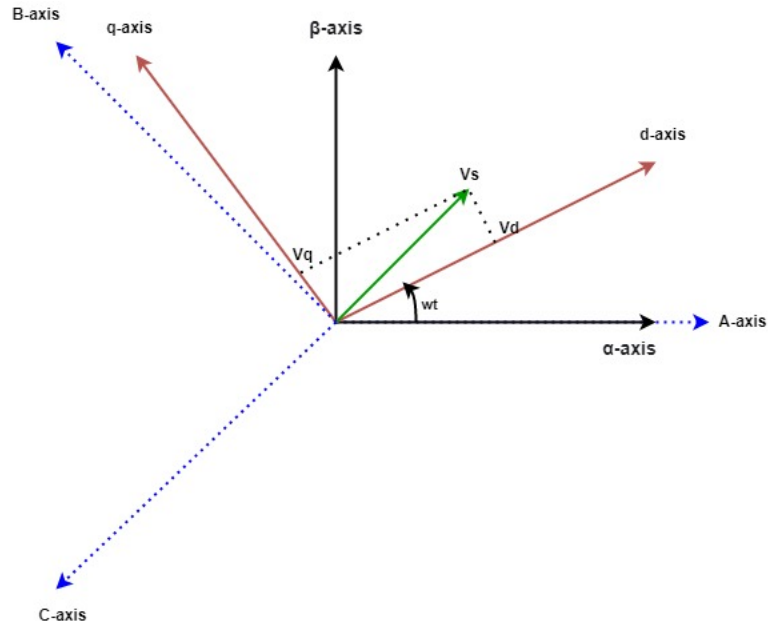


Figure 3.8: alpha-beta to dq-transformation

3.5 dq0-Frame Representation

The dq0-Frame representation, which is also called the Park transformation, is a method in which a three phase system can be represented using two rotating coordinate axis and are assumed to be under steady-state conditions. The main advantage of this transformation is to make the calculations much simpler by controlling two constants instead of three, also it has lower dynamic orders. The transformation matrices are shown in Equations (3.13) and (3.14).

$$A = \begin{bmatrix} \cos(\theta) & -\sin(\theta) & 1 \\ \cos(\theta - \frac{2\pi}{3}) & -\sin(\theta - \frac{2\pi}{3}) & 1 \\ \cos(\theta + \frac{2\pi}{3}) & -\sin(\theta + \frac{2\pi}{3}) & 1 \end{bmatrix} \quad (3.13)$$

$$A^{-1} = \frac{2}{3} \begin{bmatrix} \cos(\theta) & \cos(\theta - \frac{2\pi}{3}) & \cos(\theta + \frac{2\pi}{3}) \\ -\sin(\theta) & -\sin(\theta - \frac{2\pi}{3}) & -\sin(\theta + \frac{2\pi}{3}) \\ \frac{1}{2} & \frac{1}{2} & \frac{1}{2} \end{bmatrix} \quad (3.14)$$

It is important to mention that the zero component in the dq0-frame is the same as the zero sequence component of the voltage.

$$V_{abc} = A \times V_{dq0}, \quad (3.15)$$

$$V_{dq0} = A^{-1} \times V_{abc}, \quad (3.16)$$

In order to find the relationship between the power in the dq0-frame and in the abc frame, we need to derive the equations as follows:

$$P_{3\phi} = v_a(t)i_a(t) + v_b(t)i_b(t) + v_c(t)i_c(t), \quad (3.17)$$

$$P_{3\phi} = \begin{bmatrix} V_a & V_b & V_c \end{bmatrix} \begin{bmatrix} I_a \\ I_b \\ I_c \end{bmatrix} = \left(A \begin{bmatrix} V_d \\ V_q \\ V_0 \end{bmatrix} \right)^T A \begin{bmatrix} I_d \\ I_q \\ I_0 \end{bmatrix} \quad (3.18)$$

$$P_{3\phi} = \begin{bmatrix} V_d & V_q & V_0 \end{bmatrix} (A)^T A \begin{bmatrix} I_d \\ I_q \\ I_0 \end{bmatrix} \quad (3.19)$$

we use the following identity:

$$A^T A = \frac{3}{2} \begin{bmatrix} 1 & 0 & 0 \\ 0 & 1 & 0 \\ 0 & 0 & 1 \end{bmatrix} \quad (3.20)$$

to get

$$P_{3\phi} = \frac{3}{2} \begin{bmatrix} V_d & V_q & V_0 \end{bmatrix} \begin{bmatrix} 1 & 0 & 0 \\ 0 & 1 & 0 \\ 0 & 0 & 1 \end{bmatrix} \begin{bmatrix} I_d \\ I_q \\ I_0 \end{bmatrix} = \frac{3}{2} (V_d I_d + V_q I_q + V_0 I_0) \quad (3.21)$$

This equation describes the active power in the dq-frame. For balanced loads or three-wire systems, the zero sequence voltage will be zero. Additionally, when the synchronous frame is aligned with the voltage in the q-frame, the quadrature component equals zero. On the other hand, the reactive power will be described as follows:

$$Q_{3\phi} = \frac{3}{2} (-V_d I_q + V_q I_d + V_0 I_0) \quad (3.22)$$

In this chapter, a detailed description and calculation procedures were implemented to ensure optimum solutions with the MATLAB/Simulink model. An LC filter design was calculated and a PWM scheme was implemented. The phase locked-loop that will be later used in the grid connected mode of operation was described. A detailed calculations with numbers and optimization will be described later in Chapter 5.

CHAPTER 4:

DESIGN AND CONTROL STRATEGY

4.1 Introduction

The proposed system of Figure 4.1 consists of a DC voltage source, a VSC unit, a LC filter, a resistive critical load and a utility grid that is implemented as a distribution substation stepped down to $400V_{LL,RMS}$. The main grid is connected to the microgrid through a three-phase switch controlled by the user. When the grid is under normal operation, the three phase switch is closed and the microgrid is connected to the main utility to exchange power. This operation is called grid-connected mode. On the other hand, when the grid is under maintenance or during faults, the switch is opened and the MG is isolated from the utility to prevent any blackouts to the critical loads. The BESS will be responsible for providing the power needed to the load, as well as maintaining the source of voltage and frequency regulation of the MG. This operation is called the islanding control method.

4.2 Control Schemes

4.2.1 Grid-Connected Mode Control Scheme

Let the grid voltages be expressed as:

$$V_{sa}(t) = V_s \cos(\omega_0 t + \theta_0), \quad (4.1)$$

$$V_{sb}(t) = V_s \cos\left(\omega_0 t + \theta_0 - \frac{2\pi}{3}\right), \quad (4.2)$$

$$V_{sc}(t) = V_s \cos\left(\omega_0 t + \theta_0 + \frac{2\pi}{3}\right), \quad (4.3)$$

Where

ω_0 is the angular frequency of the grid,

V_s is the peak line to neutral voltage and

θ_0 is the phase of the source.

Transforming the sinusoidal functions into a space phasor,

$$\vec{V}_s(t) = \frac{2}{3} [e^{j0} V_a(t) + e^{j\frac{2\pi}{3}} V_b(t) + e^{j\frac{4\pi}{3}} V_c(t)] \quad (4.4)$$

and after substituting for the voltages from Equations (4.1) - (4.3) into Equation (4.4), and making use of the two following identities,

$$\cos \theta = \frac{1}{2} (e^{j\theta} + e^{-j\theta}), \quad (4.5)$$

$$0 = e^{j0} + e^{j\frac{2\pi}{3}} + e^{j\frac{4\pi}{3}}, \quad (4.6)$$

We get

$$\vec{V}_s(t) = V_s e^{j(\omega_0 t + \theta_0)} \quad (4.7)$$

Based on Equation (4.7), the space vector $\vec{V}_s(t)$ is the same as V_s which is a complex voltage that rotates counterclockwise with an angular frequency ω_0 and phase θ_0 . The only reason we are transferring from three-phase form to space phasor form is because it is simply easier to phase shift and scale a space phasor rather than a abc-frame. Examples of a space phasor representation are the $\alpha\beta$ - frame representation and the dq-frame representation. In this thesis, the dq-frame representation is used and explained briefly in Section 3.5.

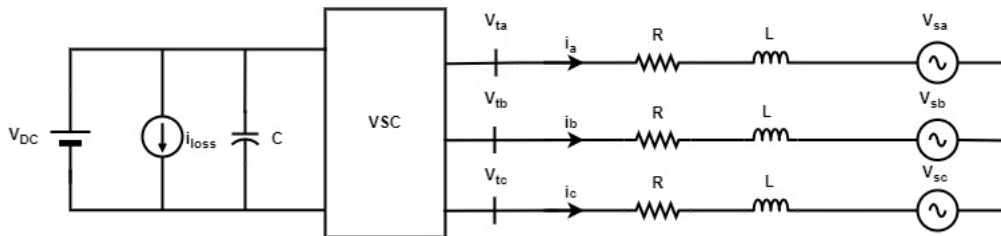


Figure 4.1: Grid-Connected Equivalent

To further investigate the behavior of the equivalent model of a microgrid of Figure 4.1, Kirchhoff's Voltage Law will be used in a per phase circuit to get the following equations:

$$L \frac{di_a}{dt} = -Ri_a + V_{ta} - V_{sa}, \quad (4.8)$$

$$L \frac{di_b}{dt} = -Ri_b + V_{tb} - V_{sb}, \quad (4.9)$$

$$L \frac{di_c}{dt} = -Ri_c + V_{tc} - V_{sc}, \quad (4.10)$$

And in order to represent them as space-phasor equation, and based on Equations (4.4) and (4.7), we obtain:

$$L \frac{d\vec{i}}{dt} = -R\vec{i} + \vec{V}_t - \vec{V}_s, \quad (4.11)$$

Where $\vec{i} = i_{dq}e^{j\rho}$ and $\vec{V}_t = V_{tdq}e^{j\rho}$ based on the following inverse transformation:

$$\vec{f}(t) = (f_d + jf_q)e^{j\rho(t)}, \quad (4.12)$$

Further information regarding the composition of the previous equations can be found in Appendix B. Then, if we substitute Equation (4.7) into Equation (4.11), and taking in mind the above dq-frame inverse transformation, we obtain:

$$L \frac{d}{dt}(i_{dq}e^{j\rho}) = -R(i_{dq}e^{j\rho}) + (V_{tdq}e^{j\rho}) - V_s e^{j(\omega_0 t + \theta_0)}, \quad (4.13)$$

Where $f_{dq} = f_d + jf_q$ for any dq quantity. When Equation (4.13) is decomposed

into real and imaginary components, we obtain:

$$L \frac{di_d}{dt} = \left(L \frac{d\rho}{dt} \right) i_q - (R)i_d + V_{td} - V_s \cos(\omega_0 t + \theta_0 - \rho), \quad (4.14)$$

$$L \frac{di_q}{dt} = - \left(L \frac{d\rho}{dt} \right) i_d - (R)i_q + V_{tq} - V_s \sin(\omega_0 t + \theta_0 - \rho), \quad (4.15)$$

To make the above equations into a space phasor representation, we need to substitute the control variable ω , where,

$$\omega(t) = \frac{d\rho}{dt}, \quad (4.16)$$

Now, Equations (4.14) and (4.15) become:

$$L \frac{di_d}{dt} = L\omega(t)i_q - (R)i_d + V_{td} - V_s \cos(\omega_0 t + \theta_0 - \rho), \quad (4.17)$$

$$L \frac{di_q}{dt} = L\omega(t)i_d - (R)i_q + V_{tq} - V_s \sin(\omega_0 t + \theta_0 - \rho), \quad (4.18)$$

If we assume that ρ has a zero initial condition, we obtain:

$$L \frac{di_d}{dt} = -(R)i_d + V_{td} - V_s \cos(\omega_0 t + \theta_0), \quad (4.19)$$

$$L \frac{di_q}{dt} = -(R)i_q + V_{tq} - V_s \sin(\omega_0 t + \theta_0), \quad (4.20)$$

But if we chose $\omega = \omega_0$ and $\rho = \omega_0 t + \theta_0$ using PLL, as described in Section 3.4,

then we conclude that the grid-connected circuit takes the dq-form representation in the following equations:

$$L \frac{di_d}{dt} = L\omega_0 i_q - (R)i_d + V_{td} - V_{sd}, \quad (4.21)$$

$$L \frac{di_q}{dt} = -L\omega_0 i_d - (R)i_q + V_{tq} - V_{sq}, \quad (4.22)$$

In this thesis, the VSC is being current-controlled (PQ control mode). This is mainly due to the tight voltage and frequency regulations of the grid. Thus, the battery system is only engaging in governing the power flow and not the frequency of the system. The proposed control strategy depends mainly on the desired active power $P_{s,ref}$. The reactive power $Q_{s,ref}$ is maintained at zero to achieve unity power factor.

Figure (4.2) shows the grid-connected control strategy and it consists of an inner current control loop and an outer power control loop when the grid is operated during normal operation and the switch is closed.

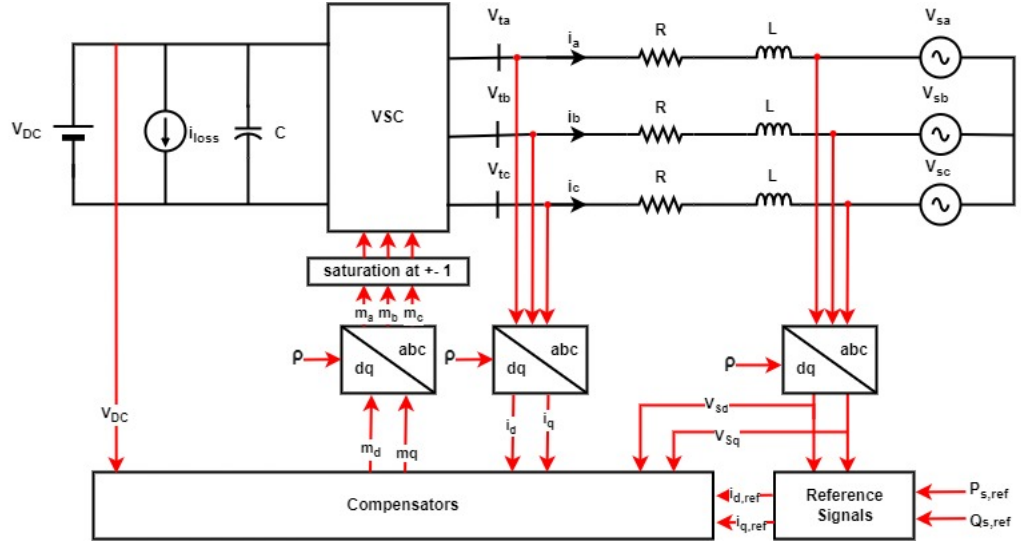


Figure 4.2: Grid-Connected Control

In order to model a two-level VSC in a dq-frame, a rather complicated long derivation is needed. For further analysis, refer to Chapter 5 in Reference [30], Where the final results are summed up by Equations (4.23) and (4.24) below,

$$V_{td}(t) = \frac{V_{DC}}{2}m_d(t), \quad (4.23)$$

$$V_{tq}(t) = \frac{V_{DC}}{2}m_q(t), \quad (4.24)$$

where $m_d(t)$ and $m_q(t)$ are the modulation indices of the PWM scheme in the dq-frame. Also, they are considered very important in our simulation when they are both transformed to the abc-frame in order to be appropriately used for a two-level VSC (refer to Section 3.2). In Equations (4.22) and (4.23), the $L\omega_0$ term makes i_d and i_q dynamically coupled.

However, we are interested to control each current on its own. That means we should decouple the behavior of i_d from that of i_q . In order to achieve this decoupling, we determine m_d and m_q are, as a function of new control inputs u_d and u_q .

$$m_d = \frac{2}{V_{DC}}(u_d - L\omega_0 i_q + V_{sd}), \quad (4.25)$$

$$m_q = \frac{2}{V_{DC}}(u_q + L\omega_0 i_d + V_{sq}), \quad (4.26)$$

If we substitute Equations (4.25) and (4.26) into (4.23) and (4.24), and substituting (4.21) and (4.22), we deduce that,

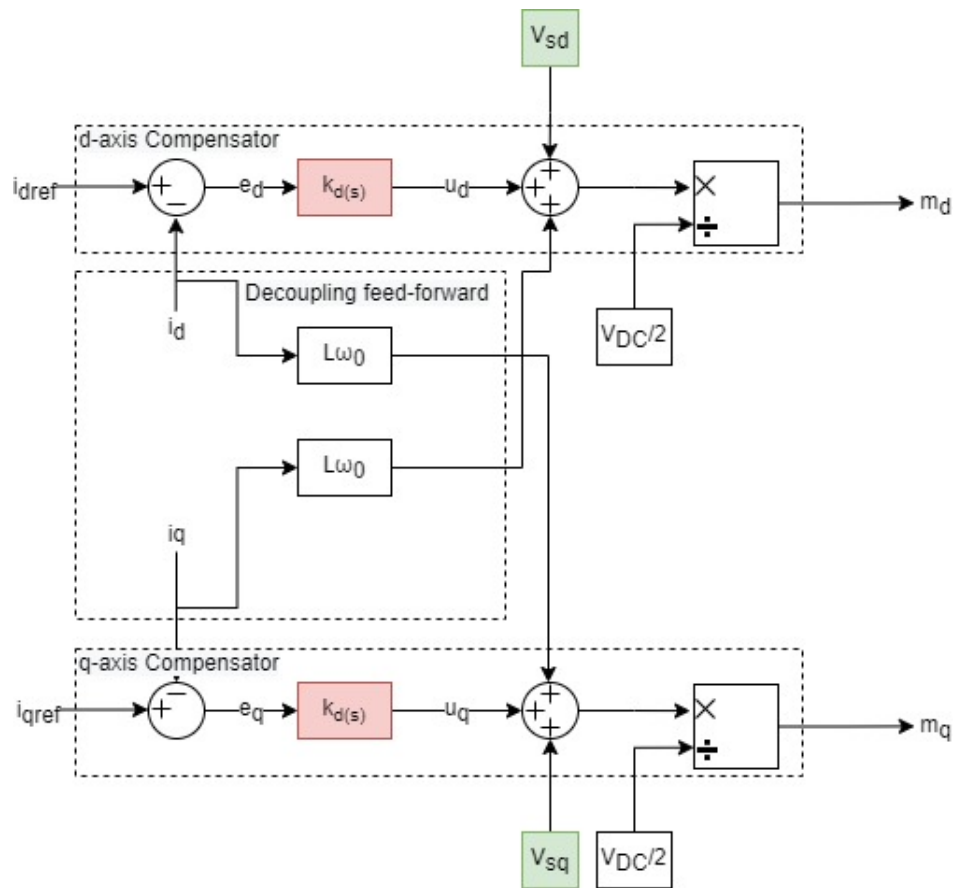


Figure 4.3: Control Block Diagram of a current controlled VSC system

$$L \frac{di_d}{dt} = -(R + r_{on})i_d + u_d, \quad (4.27)$$

$$L \frac{di_q}{dt} = -(R + r_{on})i_q + u_q, \quad (4.28)$$

In the previous equations, it is clear that the currents i_d and i_q are now decoupled, which means that we have achieved our goal.

Figure 4.3 shows a block schematic diagram that represents the current-controlling scheme in the dq-frame representation. The errors e_d and e_q are the differences between the currents at the point of common coupling (PCC) and the reference current. Compensators are needed to calculate the new control inputs u_d and u_q . Then based on Equations (4.25) and (4.26), the modulation indices of the PWM are generated through u_d and u_q by adding the corresponding PCC voltages in the dq-frame. The $L\omega_0$ terms are multiplied by the currents at the PCC. The resultant value is then multiplied by $\frac{2}{V_{DC}}$ to get m_d and m_q .

One of the most important advantages of using a dq-frame rather than an abc-frame or $\alpha\beta$ -frame is that the calculation process for the PID controller compensators is fairly easy because they are at low dynamic orders. Let k_d , k_p and k_i be defined as follows [31],

$$k_d(s) = \frac{k_p s + k_i}{s}, \quad (4.29)$$

$$k_p = \frac{L}{\tau_i}, \quad (4.30)$$

$$k_i = \frac{(R + r_{on})}{\tau_i} \quad (4.31)$$

Where τ is a design perimeter of choice. It should be fairly small to result in a fast current-control response but adequately large so that the bandwidth of the closed-loop control system is much smaller than $\frac{1}{\tau}$. It is typically chosen between 0.5-5ms.

4.2.2 Islanded Mode Control Scheme

The main objective of having an islanded mode of operation is to provide a backup supply of power when the main utility grid is under maintenance or during faults. This operation is important to be stable and to be available at all times for urgent facilities and emergency loads, such as hospitals. When studying the controls of this mode of operation, unlike during grid-connected mode, a filter capacitor C_f is needed to ensure a smoother voltage behavior. A capacitance is known for its ability to provide voltage support and less harmonics and noise. The smart inverter is acting as a voltage-controlled VSC, which means that the inverter is controlling the voltage of the microgrid and maintaining the frequency at an acceptable and stable value.

In this thesis, the frequency will be supplied by the inverter through a signal generator that is generating a periodic scalar signal having a waveform that was specified using a time values of zero to $1/60$ of an amplitude of zero and 2π , respectively. The reason for generating a frequency signal is due to the low inertia of DERs compared to the main grid. Because the system finds it hard to maintain the frequency of the MG, the smart inverter acts like a frequency-controlled VSC [32]. The controlling part is implemented in the dq-frame, as previously shown in the grid-connected mode of operation.

In this section, we first will represent a dq-frame model for the voltage-controlled system, as shown in Figure 4.4, and then briefly explain the operation of the control strategy of the VSC, as shown in Figure 4.5.

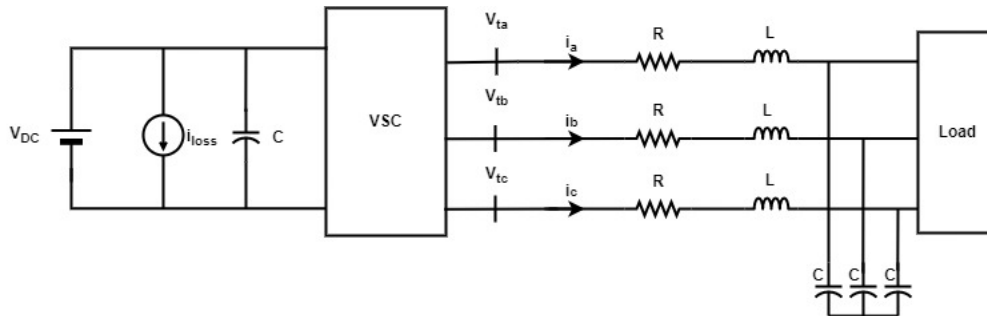


Figure 4.4: Islanded Mode Equivalent

The objective of our derivation is to control the behavior of the smart inverter in the islanded-mode without a prior knowledge of the load model. This can be carried out through a feedforward compensator that will eventually decouple the load dynamics from our smart inverter system. On the other hand, the active and reactive power are not controlled by the inverter controller anymore. Instead a reference voltage signal is imposed as a base value for the calculations.

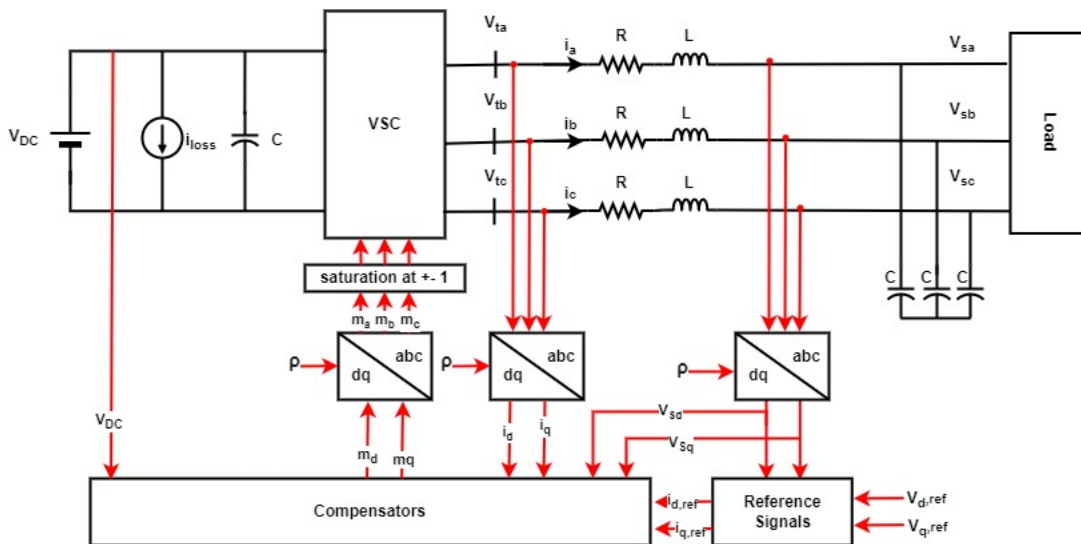


Figure 4.5: Islanded Mode schematic

In Figure 4.5, I_{dref} should be optimized based on a predetermined V_{dref} . This

can be achieved by setting the reference voltage at the peak value of the grid. Equations (4.32) and (4.33) describe the relationship between the reference current and the load current:

$$C_f \frac{dV_{La}}{dt} = i_a - i_{La}, \quad (4.32)$$

$$C_f \frac{dV_{Lb}}{dt} = i_b - i_{Lb}, \quad (4.33)$$

$$C_f \frac{dV_{Lc}}{dt} = i_c - i_{Lc}, \quad (4.34)$$

Transforming Equations (4.32) through (4.34) to dq-form will result in the following:

$$C_f \frac{dV_{Ld}}{dt} = C_f \omega V_{Ld} + i_d - i_{Ld}, \quad (4.35)$$

$$C_f \frac{dV_{Lq}}{dt} = -C_f \omega V_{Lq} + i_q - i_{Lq}, \quad (4.36)$$

In order to eliminate the coupling between V_{Ld} and V_{Lq} , a feedforward compensator system similar to the one used for the grid-connected mode is used. This will make it possible to regulate V_{Ld} by I_{dref} and V_{Lq} by I_{qref} , as expressed in the following:

$$i_{dref} = u_d - C_f(\omega V_{sq}) + i_{Ld}, \quad (4.37)$$

$$i_{qref} = u_q + C_f(\omega V_{sd}) + i_{Lq}, \quad (4.38)$$

The optimum solution will be as follows:

$$i_{dref} = i_d - j\omega C_f V_q, \quad (4.39)$$

$$i_{qref} = i_q - j\omega C_f V_d \quad (4.40)$$

A cascaded solution has been implemented in the islanded-mode of operation, as described in Figure 4.5:

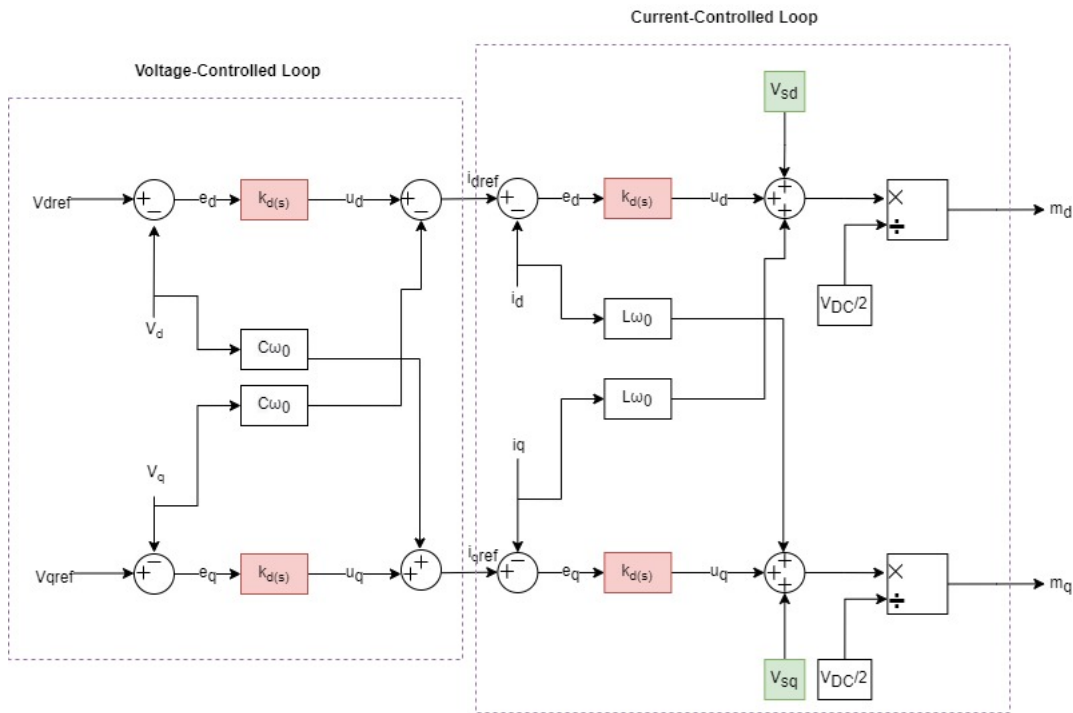


Figure 4.6: Islanded Mode Cascaded Solution

4.2.3 Transition Mode Control Scheme

As previously discussed, the main objective of doing this research is to achieve a seamless transition between grid-connected mode and islanding mode. The transitioning from grid-connected mode to islanding mode is called islanding and the transition from islanding mode to grid-connected mode is called de-islanding. Deviations and transients in voltages and currents appear during these sudden transitioning times due to the existence of switching devices and load dynamics. The re-synchronization to the grid after being in islanding mode can be complicated, but it is surely important. Figure 4.7 describes the switching between the two modes of operation,

where in Islanded mode the switch will be at the zero state (0), that will allow a two loop operation to be implemented, first the voltage-controlled loop and second the current-controlled loop. In grid-connected mode, the switch will be at the one state (1) which means only one loop will be in operation which is the current-controlled loop.

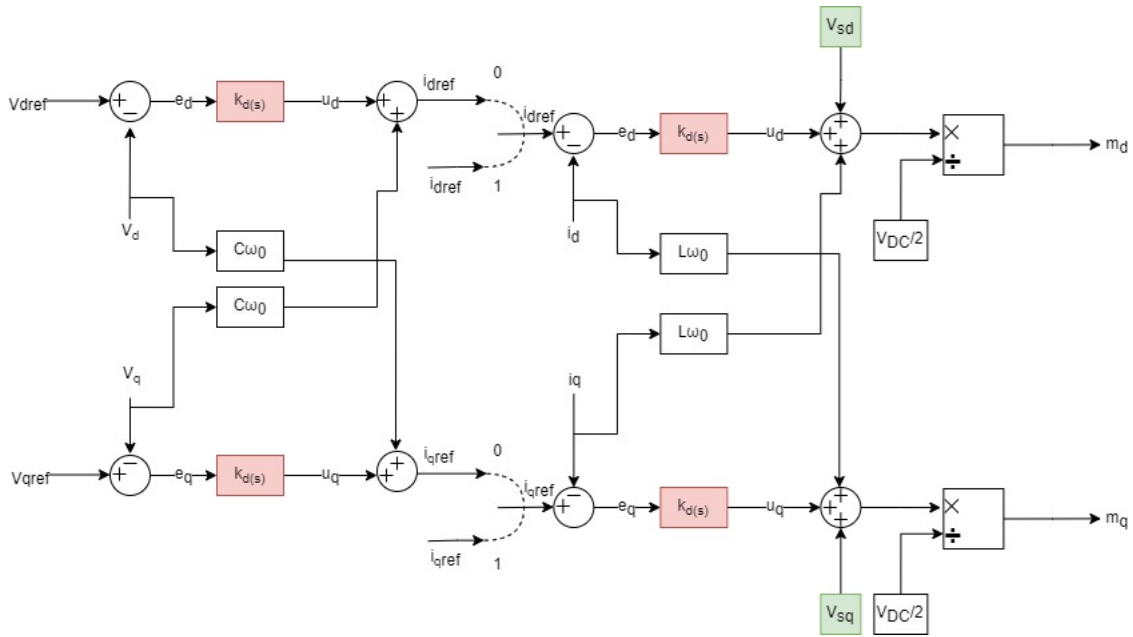


Figure 4.7: Seamless transition Solution

4.3 Fault Detection

After discussing each control system on its own, it is important to consider a system that can function in both modes of operation. Moreover, the smart inverter should be able to detect any disruptions or faults on the grid, so that it can take a decision to isolate as fast as possible during unintentional islanding.

In Figure 4.8, PCC is the point where the load, the VSC filter output and the grid share. The inverter is sharing a communication link with the grid. This enables

the smart inverters (VSC) to sense any variations on the grid side by the continuous shared set points of currents and voltages. If the inverter senses any deviations from the predefined threshold values, it will send a signal to the bypass switch to force it to open. During this instance of time, the smart inverter changes from the current-controlled mode to the voltage-controlled mode. The voltage and frequency limits and the threshold have been explained in section 2.4. If the grid has been maintained to the original healthy state and all faults has been cleared, the inverter will send a signal to the bypass switch to close after synchronization with the grid using the PLL, refer to Figure 4.9.

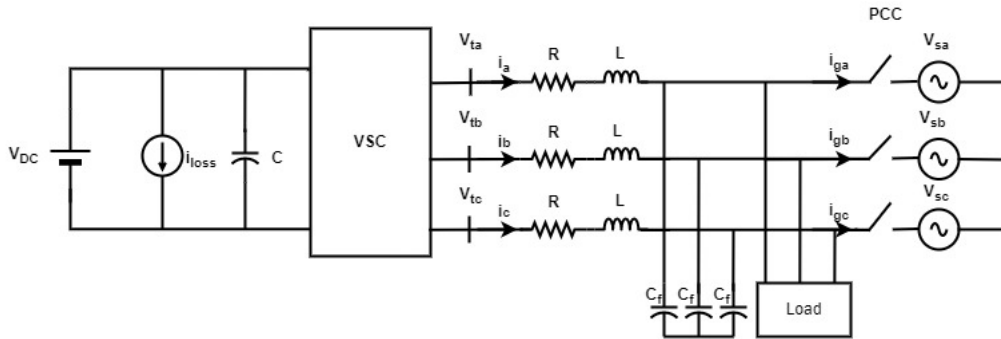


Figure 4.8: Fault Detection

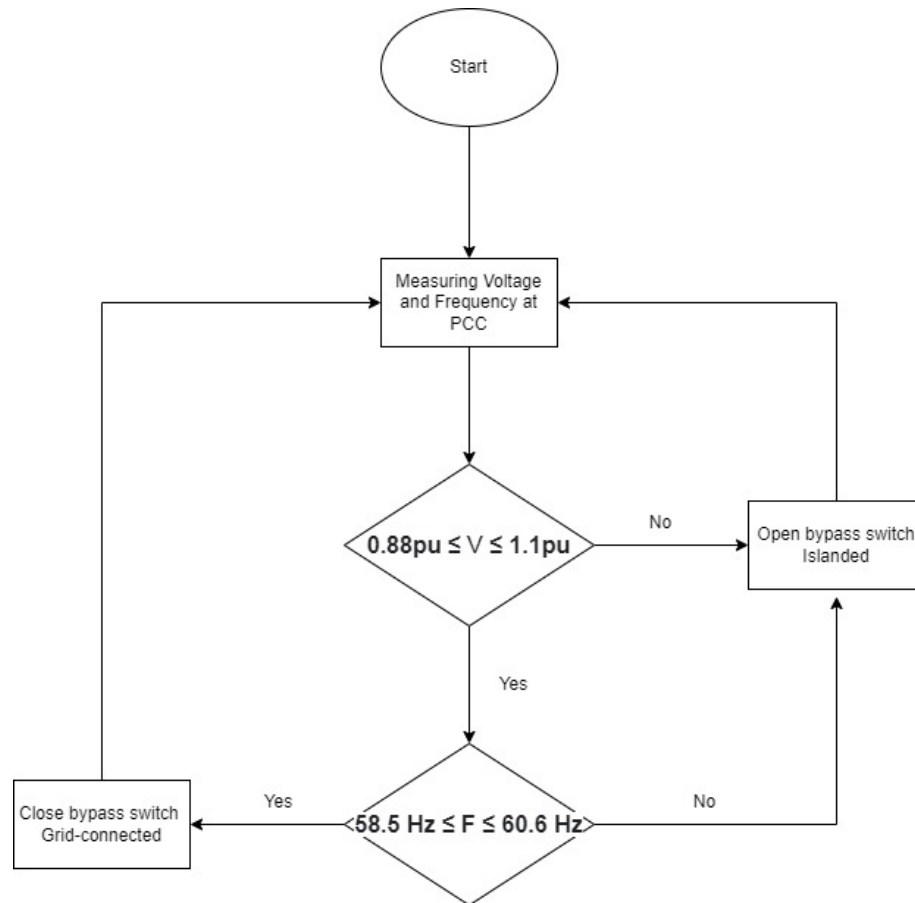


Figure 4.9: Flowchart of Fault Detection Criteria

In this chapter, we discussed the three control schemes; grid-connected mode, islanded mode and transition mode of operation. We designed a fault detection scheme that was explained through a flowchart.

CHAPTER 5:

RESULTS

5.1 Introduction

In the previous chapter, three detailed control schemes were explained and illustrated with block diagrams. In this chapter, multiple simulations were implemented using the Simulink/MATLAB software to investigate the behavior of the microgrid and its synchronization with the grid. The microgrid should be sharing and receiving purely sinusoidal voltages and currents with the grid with acceptable harmonics and noise level. Also, an automatic fault detection should be clever enough to make a decision based on the grid voltage and frequency. The system should go to the islanded mode when the voltage and the frequency of the grid is out of the acceptable range of the IEEE 1547-2018 standard. The transition between the two states should be smooth and with minimal noise and transients, to avoid damaging the equipment and loads. The simulations provided in this chapter include a BESS with no PV system, to emphasize the behavior of a DC source in a microgrid, which also can be modeled as a PV. The grid parameters are based on a low-voltage distribution system, as shown in Table 5.1. It is important to mention that in the Electrical Engineering field, the grid voltage is always specified line-to-line and in effective (RMS) values.

5.2 Design Parameters

In this section, I will calculate the parameters used in this design and try to optimize the numbers to get better results using different values for the time constant.

5.2.1 Grid Parameters

In this model, the three-phase source used is shown in Figure 3.1, with the following values:

Table 5.1: Grid Parameters

Parameter	Value
Grid Voltage (V_s)	400 V
Grid Frequency (F_s)	60 Hz
Grid Resistance (R_s)	$1\mu\Omega$
Grid Inductance (L_s)	10^{-12}H

5.2.2 Inverter Parameters

In this thesis, a two-level three phase 100 kVA VSC is used. The design includes 6 IGBTs, and each of them has a snubber resistance, internal resistance and a snubber capacitance. Table 5.2 summarizes the IGBT parameters of the inverter used. For the PWM, a comparator is used for each phase modulation index with a repeating high-frequency periodic triangular waveform signal (carrier signal) with a frequency of 10 kHz.

Table 5.2: IGBT of VSC Parameters

Parameter	Value
Snubber Resistance ($R_{snubber}$)	100k Ω
Snubber Capacitance Capacitance (C)	infinity
On Resistance (R_{on})	1m Ω

5.2.3 LC filter Parameters

The LC filter values used based on the simulation design and optimizing using Equations 5.1 to 5.3 are summarized in Table 5.2.

Table 5.3: The LCL Filter Parameters

Parameter	Value
Filter Inductance (L)	1mH
Filter Capacitance (C)	100 μ F

To calculate the filter capacitance, we use Equations (3.8) and (3.9) to write that:

$$Q = \frac{V^2}{X_c} = \frac{V^2}{1/(2\pi fC)} \quad (5.1)$$

If we reshuffle the variables in order to get the capacitance, and knowing that as a thumb rule, the reactive power absorbed by the capacitor is 0.05 of the rated apparent power (S) of the system, we get,

$$C = \frac{0.05S}{V^2 2\pi f} = \frac{0.05 \times 100}{\sqrt{3} \times 400^2 \times 2 \times \pi \times 60} = 84 \times 10^{-6} F \quad (5.2)$$

For design purposes, I used $C = 100 \mu\text{F}$.

To calculate the filter inductance, we can either use Equation (3.10) or (3.11). In my design, I chose Equation (3.11) by calculating the following:

$$L = \frac{0.2V_g}{2\pi fI} = \frac{0.2 \times 400}{2 \times \pi \times 60 \times 144}, \quad (5.3)$$

for design purposes, I used $L = 1 \text{ mH}$.

To make things less complicated, a list of acronyms are provided in Table 5.4.

Table 5.4: Design Acronyms

Parameter	Acronym
Grid Voltage	V_s
Grid Current	I_s
Grid Frequency	F_s
Inverter Terminal Voltage	V_T
Inverter Terminal Current	I_T
Inverter Terminal Frequency	F_T
Load Voltage	V_L
Load Current	I_L
Load Frequency	F_L

The simulation time was chosen as 1 second, in order to minimize the simulation time. The powergui used in this analysis is a discrete type, with sampling time of 10^{-6} s. The first simulation was conducted in a grid-connected mode without any faults on the grid. Another simulation was implemented for 1 second, where a fault was conducted on the grid side at 0.1 seconds and then the fault was isolated at 0.2 seconds. During that time, the detection scheme should be able to detect

the disruption on the grid voltage, and send a command to the bypass switch to isolate the microgrid and ensure continuous power supply to the critical load. This also means that the control system should switch from current-controlled mode to voltage-controlled mode without significant transients. On the other hand, when the fault is isolated, the detection scheme should send an automatic command to the bypass switch to close after the frequency and voltage transients have been smoothed out, using a PLL.

5.3 Grid-Connected Simulation

For ease of reference, Figure 4.2 will be illustrated again in this chapter as Figure 5.1. A control scheme is applied to the system in order to regulate the operation of the microgrid when it is connected to the grid. In other words, the amount of power ($P_{s,ref}$) and reactive power ($Q_{s,ref}$) shared between them should be predetermined based on the inverter size.

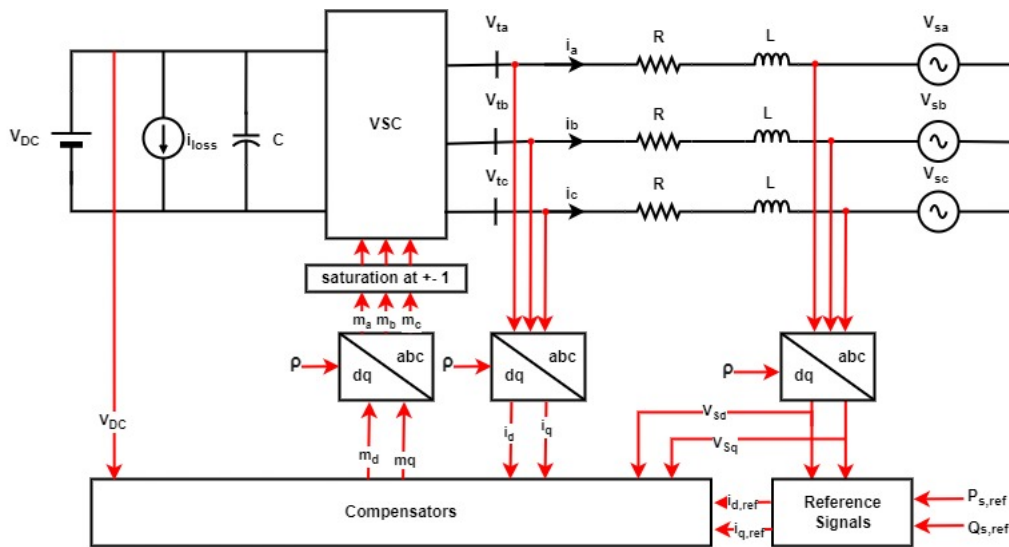


Figure 5.1: Grid-Connected Control

A 100-kVA inverter with a unity power factor is used to determine the reference current ($I_{d,ref}$) in the grid-connected mode, based on Equation (5.4).

$$I_{d,ref} = \frac{S_{3ph}}{\sqrt{3} V_s} = \frac{100}{\sqrt{3} 400} = 205A \quad (5.4)$$

On the other hand, ($I_{q,ref}$) will be set to zero, to support a zero reactive power supplied by the inverter. The frequency (f_s) and voltage (V_s) with this scheme are imposed by the grid. Thus, the three-phase voltages setpoints from the grid side will be transposed using a dq0-transformation, mentioned in Section 3.5, and fed into a compensator. The setpoints of the inverter terminal three-phase currents are transformed into the dq0 scheme and also fed back to the compensator. The compensator is achieved using Equations (4.25) and (4.26). The PLL takes setpoints for the grid voltages at the PCC and locks V_q to zero, therefore locking the inverter voltage to the grid voltage with the same phase. As long as the grid voltage V_s magnitude is within the acceptable range, then the bypass switch will stay closed and connected to the microgrid.

Figure 5.2 shows sinusoidal grid voltages with a peak value of $V_s\sqrt{2}$ and with currents in a three-phase sinusoidal steady-state. Figure 5.3 shows the grid frequency stabilizing after 0.2 seconds at 60 Hz. Figure 5.4 shows the inverter terminal voltage V_t and i_t , after filtering out all the harmonics using the LC filter. Figure 5.5 shows the load voltage V_L and I_L , in a sinusoidal form after trying out several values for the K_p and K_i associated with the PID controllers.

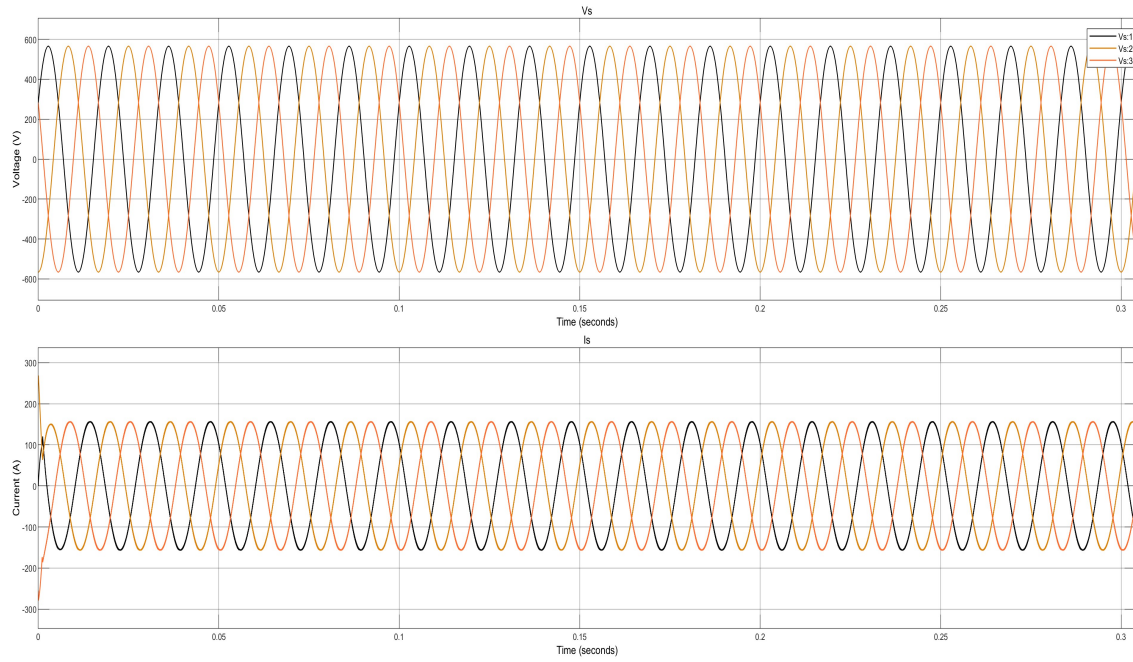


Figure 5.2: Grid Voltage (V_s) and Current (I_s) in Grid-Connected mode

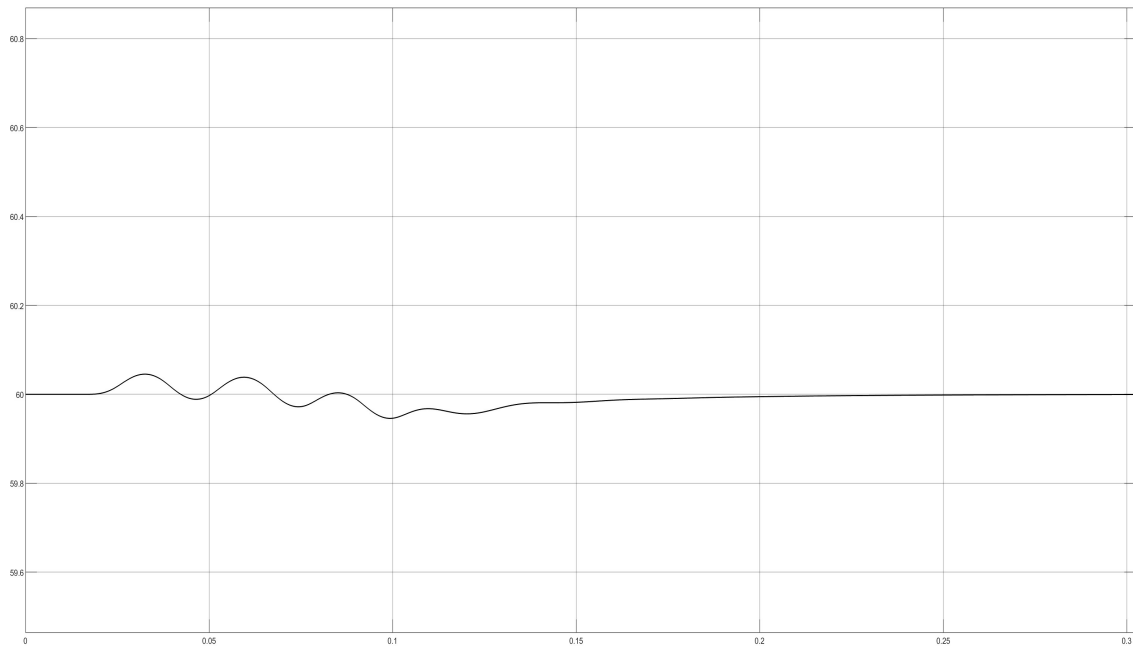


Figure 5.3: Grid Frequency in Grid-Connected mode

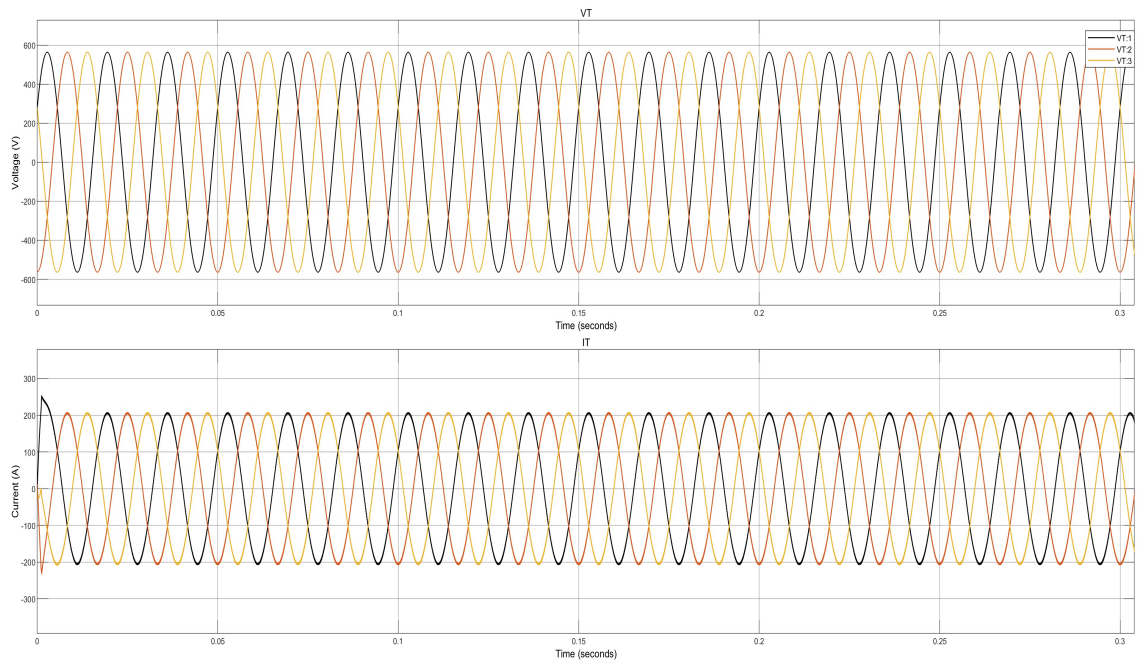


Figure 5.4: Inverter Terminal Voltage (V_T) and Current (I_T) in Grid-Connected Mode

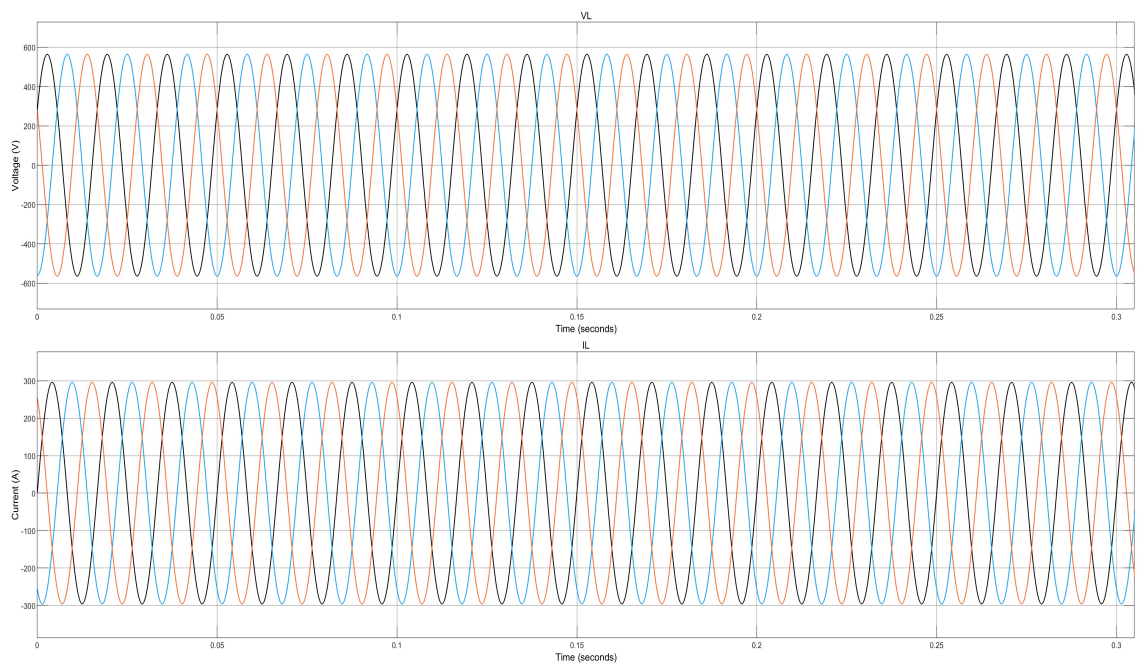


Figure 5.5: Load Voltage (V_L) and Current (I_L) in Grid-Connected Mode

5.4 Islanded Simulation

For ease of reference, Figure 4.5 will be illustrated again in this chapter as Figure 5.6. When the grid is experiencing intentional islanding due to faults or maintenance, the bypass switch opens automatically or manually, to avoid a blackout of the critical loads in the microgrid. At this stage, the microgrid has no reference voltage or frequency imposed by the grid. Instead, the frequency will be supplied by a repeating sequence source that has a fixed frequency of 60 Hz. The inverter will be functioning as a voltage-controlled VSC, which means the voltage of the microgrid will be imposed by the inverter, using the normal peak value of the grid voltage $V_{d,ref} = 400\sqrt{2}$. In this case, $V_{q,ref}$ will be set to zero, to put the inverter at unity power factor. The load voltage is taken as a setpoint for the compensator calculations after transforming them from three-phase values to dq values. This process is called the voltage control loop. The output reference currents from this loop will be used as an input for the current control loop in the same process used for the grid-connected scheme. The method used is a cascaded control scheme that will operate both loops only in the case of an islanding mode of operation but will only operate the current loop in the case of grid-connected mode.

The second simulation is being implemented at this scheme, where a symmetrical fault is established at the grid PCC at 0.1 seconds. Therefore, the detection scheme is able to detect the voltage drop and open the switch automatically. At the same instance, the cascaded control scheme changed from only operating the voltage control loop to operating both loops. Figure 5.7 shows the voltage and current at PCC. It is clear that the system was operating in grid-connected mode for the first 0.1 second, with the frequency being imposed by the grid. At time 0.1 second, the voltage drops

at the PCC, because it would be the same as the voltage across the load. The current is clearly zero in that stage, to show that the switch is open and no power is being shared with the grid. At time 0.2 seconds the fault is cleared and the current is back to normal. Figure 5.8 shows that the frequency transients are within the acceptable limits of the IEEE 1547-2018 standard. Figure 5.9 shows the inverter terminal voltage and currents, where the inverter is contributing with a higher current during the islanded mode to cover the loss of the grid. Lastly and most importantly, Figure 5.10 shows the load voltages and currents during the transition period. This transition is very smooth and seamless, which means that there are minimal transients that would damage the equipment.

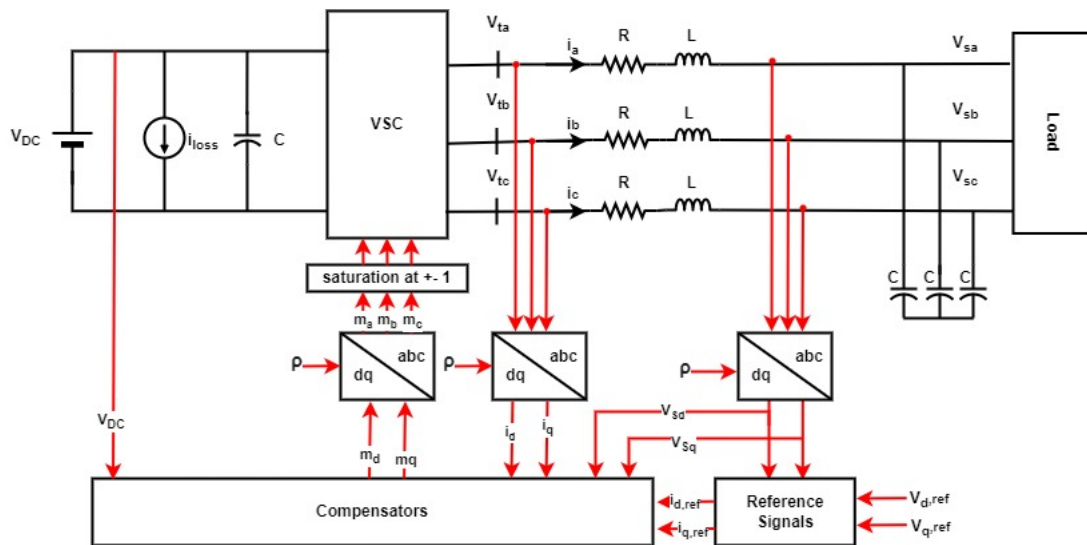


Figure 5.6: Islanded Mode schematic

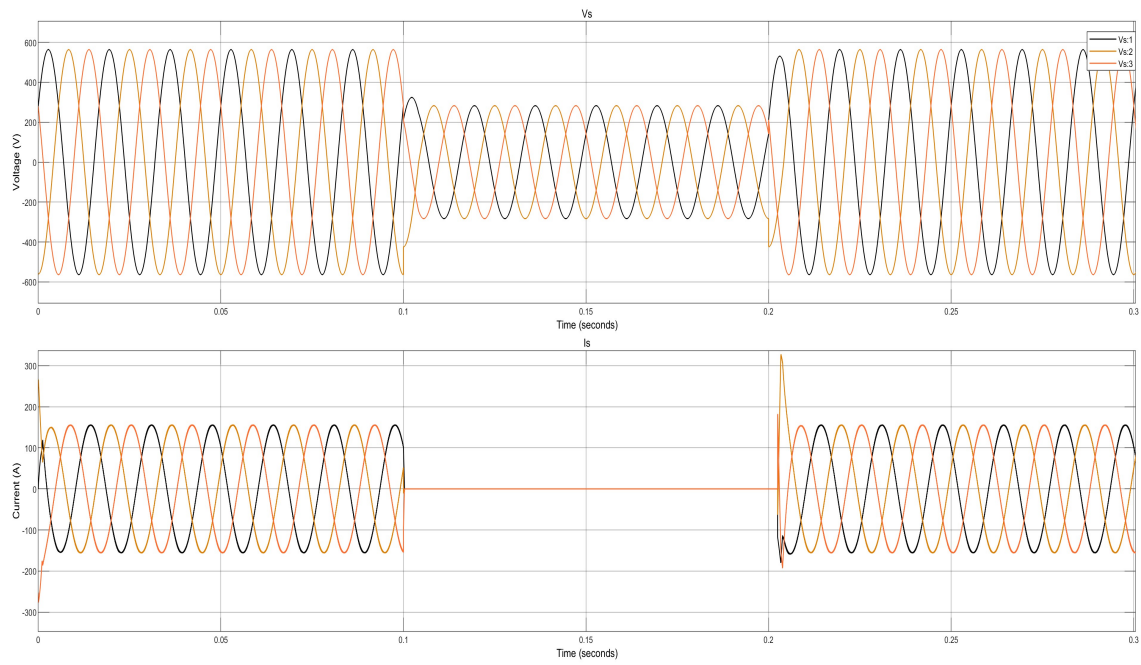


Figure 5.7: Grid Voltage (V_s) and Current (I_s) in Islanded mode

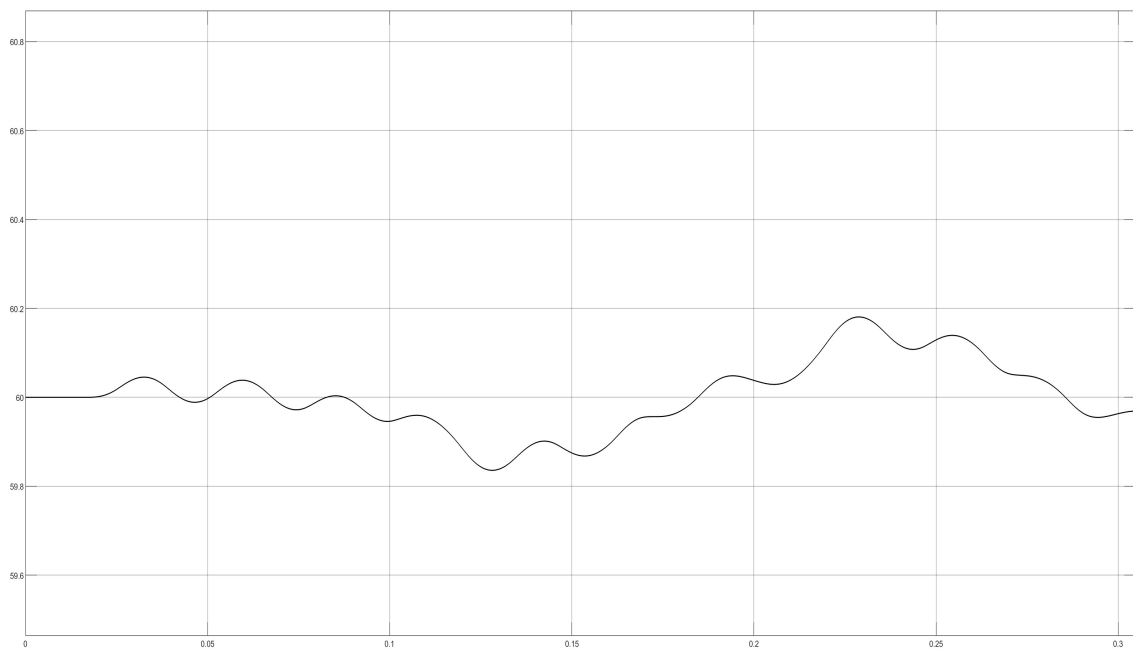


Figure 5.8: Grid Frequency in Islanded mode

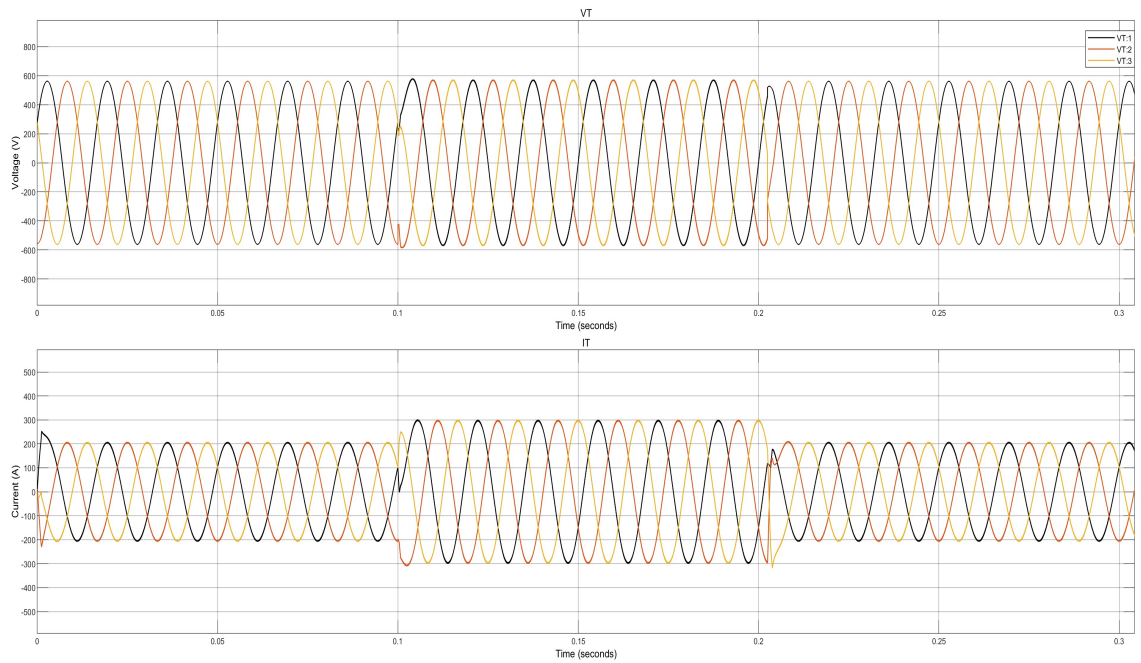


Figure 5.9: Inverter Terminal Voltage (V_T) and Current (I_T) in Islanded Mode

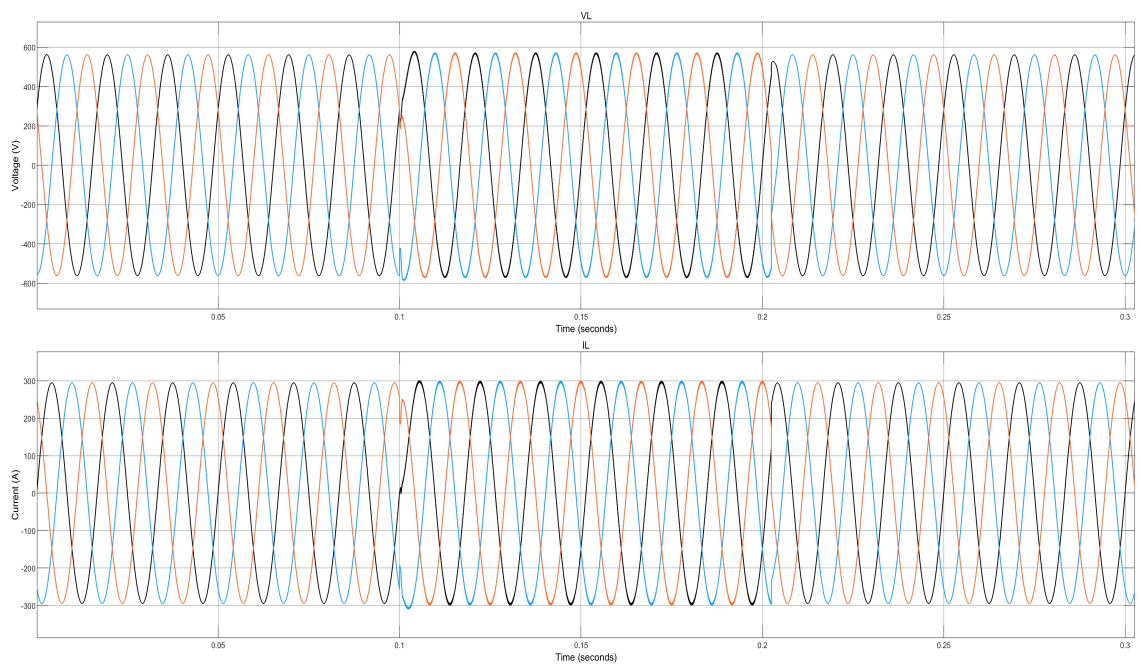


Figure 5.10: Load Voltage (V_L) and Current (I_L) in Islanded Mode

5.5 Self-Detection Simulation

The system is required to work in both modes of operation and, in order to achieve that, an automatic fault detection scheme is simulated, as shown in Figure 5.11. If we assume the system is healthy and the inverter is sharing power with the load and the grid, then the detection scheme that calculates the voltage magnitude will have the results within an acceptable range. Otherwise, if a fault happens on the grid side, then the voltage magnitude will drop and the detection scheme calculating the voltage magnitude using Equation (5.5) will be out of range.

$$V_s = \sqrt{V_\alpha^2 + V_\beta^2} \quad (5.5)$$

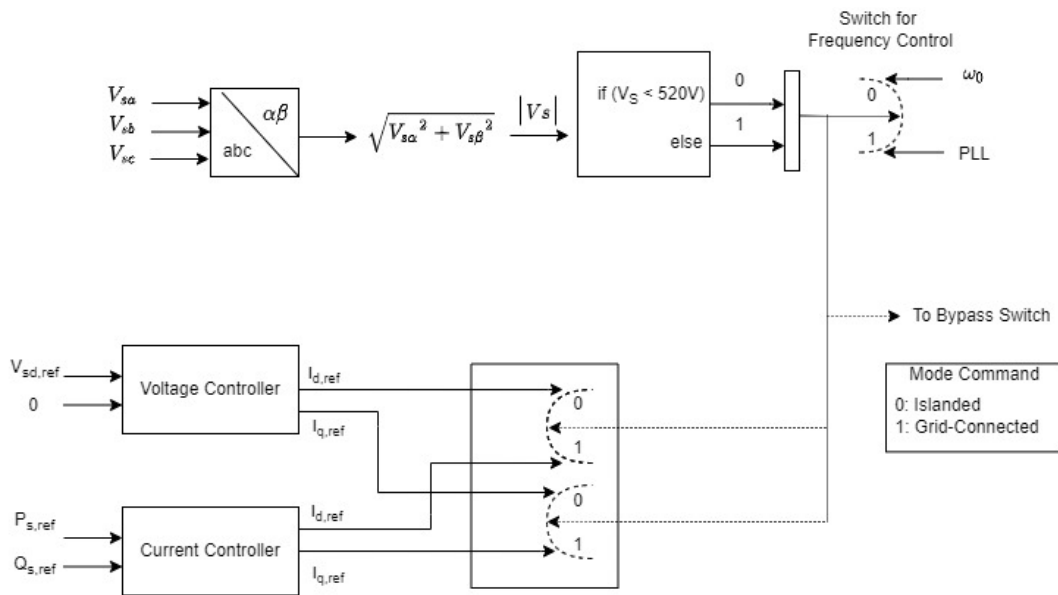


Figure 5.11: Switching Scheme

As a result, a mode command was sent to both the frequency control switch and control switch, as well as the main bypass switch. The frequency was shifted from

being controlled by the PLL to being imposed by the inverter. The control scheme switched from the current-controlled scheme to the voltage-controlled scheme. Finally, the bypass switch opened and as a result, the microgrid was isolated from the main grid and started functioning autonomously.

CHAPTER 6:

CONCLUSIONS AND FUTURE WORK

6.1 Conclusions

In the previous chapter, we tested the performance of a fast control system to provide a seamless transition between grid-connected and islanded mode and validated the results simulation with graphs. We also detailed the calculations used to design the various elements in the power system. Subsequently, a BESS system was implemented to represent the renewable energy penetration in the microgrid. A resistive load was being used as the critical load.

Two simulations were implemented: the first one is a healthy system working in grid-connected mode. The results shown in Figures 5.2 to 5.5 prove that the control scheme in the current-controlled mode of operation is functioning. The VSC is sharing power with the load and the grid based on the reference current given. The frequency of the VSC is being imposed by the grid and synchronized with the grid, and it is fluctuating within the acceptable range of the IEEE 1547-2018. The reactive power supplied by the inverter is zero, due to imposing a unity power factor on the inverter. The second simulation was implemented with 0.1 seconds duration of a fault on a grid before it was cleared. The voltage-controlled scheme was able to provide smooth power to the load and the VSC was able to impose the voltage and

the frequency to the MG. Figures 5.7 to 5.10 show filtered sinusoidal waveforms for the voltage and the currents at different locations of the microgrid. The designed LC filter provided a smooth signal with minimal harmonics.

The main purpose of this thesis was met with the cascaded designed system between the current-controlled and voltage-controlled scheme by providing a PLL scheme that was able to quickly synchronize the microgrid with the utility grid after reclosing the bypass switch. The hybrid detection scheme was able to detect a symmetrical fault on the grid and automatically isolate the microgrid to prevent any blackouts on the critical load. To sum up, the IEEE1547-2018 standards for voltage and frequency mandatory tripping and ride-through requirements were met by the detection scheme.

6.2 Future Work

In the future, the proposed control scheme can be further developed to make the system more reliable, more economical and secure. This includes but is not limited to the following:

1. Integrating a wider variety of DERs such as diesel generators, PV power plant and wind turbines.
2. The load can be extended to dynamic and constant distributed loads, including inductive and resistive loads.
3. In the near future, the plan is to accommodate the proposed control scheme to cover unsymmetrical faults alongside the symmetrical faults. This way, the simulation will be more practical and closer to real life control schemes. A way to tackle this problem is to provide a detection scheme based on comparing the

symmetrical components of the system using logic gates and filters.

4. Another useful investigation would be managing the battery energy management system using the smart features of the inverter to include examining the state of charge of the battery and making a decision based on the lifetime of the battery.
5. Also, the communication links between the inverters and the grid will be further analyzed to make the system capable of isolating when the communication links are lost due to weather conditions or any sort of hazards.
6. Faults at different locations of the power systems, including feeder locations, can be examined more closely to see the behavior of the inverter.
7. Furthermore, protection devices, such as relays, could be added to the system to isolate any faults quickly. This will make the system more comprehensive and more reliable.
8. As the world is becoming less secure, a cybersecurity scheme can be developed on the critical infrastructure of the system using IEC 62443-Industrial Security Standards to prevent threats on operational technology that are internet-connected. The smart inverters are more prone to these attacks because they use communication links to regulate the voltage and the frequency. A cybersecurity system can make the system more secure against attacks.

REFERENCES

- [1] Hannah Ritchie Max Roser and Esteban Ortiz-Ospina. World population growth. *Our World in Data*, 2013. <https://ourworldindata.org/world-population-growth>.
- [2] Xiaoling Jin. Analysis of microgrid comprehensive benefits and evaluation of its economy. In *10th International Conference on Advances in Power System Control, Operation Management (APSCOM 2015)*, pages 1–4, 2015.
- [3] Mike Quashie and Geza Joos. A methodology to optimize benefits of microgrids. In *2013 IEEE Power Energy Society General Meeting*, pages 1–5, 2013.
- [4] Usman Bashir Tayab, Junwei Lu, Seyedfoad Taghizadeh, Ahmed Sayed M. Metwally, and Muhammad Kashif. Microgrid energy management system for residential microgrid using an ensemble forecasting strategy and grey wolf optimization. *Energies*, 14(24), 2021.
- [5] Yinliang Xu and Xinwei Shen. Optimal control based energy management of multiple energy storage systems in a microgrid. *IEEE Access*, PP:1–1, 06 2018.
- [6] Cheng Jin, Mingzhi Gao, Xiaofeng Lv, and Min Chen. A seamless transfer strategy of islanded and grid-connected mode switching for microgrid based on droop control. In *2012 IEEE Energy Conversion Congress and Exposition (ECCE)*, pages 969–973, 2012.

- [7] Xiaochao Hou, Yao Sun, Jinghang Lu, Xin Zhang, Leong Hai Koh, Mei Su, and Josep M. Guerrero. Distributed hierarchical control of ac microgrid operating in grid-connected, islanded and their transition modes. *IEEE Access*, 6:77388–77401, 2018.
- [8] Ashraf Khalil, Khalid Ateea Alfaitori, and Ali Asheibi. Modeling and control of pv/wind microgrid. In *2016 7th International Renewable Energy Congress (IREC)*, pages 1–6, 2016.
- [9] Ieee standard for the specification of microgrid controllers. *IEEE Std 2030.7-2017*, pages 1–43, 2018.
- [10] Fahmid Sadeque, Dushyant Sharma, and Behrooz Mirafzal. Power-sharing between grid-forming and grid-following inverters. In *2021 IEEE 22nd Workshop on Control and Modelling of Power Electronics (COMPEL)*, pages 1–5, 2021.
- [11] Behrooz Mirafzal and Aswad Adib. On grid-interactive smart inverters: Features and advancements. *IEEE Access*, PP, 09 2020.
- [12] Mehrdad Yazdanian and Ali Mehrizi-Sani. Distributed control techniques in microgrids. *IEEE Transactions on Smart Grid*, 5(6):2901–2909, 2014.
- [13] Ieee standard for interconnection and interoperability of distributed energy resources with associated electric power systems interfaces. *IEEE Std 1547-2018 (Revision of IEEE Std 1547-2003)*, pages 1–138, 2018.
- [14] F. Noor, R. Arumugam, and M.Y. Vaziri. Unintentional islanding and comparison of prevention techniques. pages 90 – 96, 11 2005.

- [15] Mohit Kumar Sharma, Praveen Kumar, and Vishal Kumar. Intentional islanding of microgrid. In *2017 6th International Conference on Computer Applications in Electrical Engineering-Recent Advances (CERA)*, pages 247–251, 2017.
- [16] Abhisek Mishra and Premalata Jena. A scheduled intentional islanding method based on ranking of possible islanding zone. *IEEE Transactions on Smart Grid*, 12(3):1853–1866, 2021.
- [17] J.A.P. Lopes, C.L. Moreira, and A.G. Madureira. Defining control strategies for microgrids islanded operation. *IEEE Transactions on Power Systems*, 21(2):916–924, 2006.
- [18] Ali Mehrizi-Sani and Reza Iravani. Potential-function based control of a microgrid in islanded and grid-connected modes. *IEEE Transactions on Power Systems*, 25(4):1883–1891, 2010.
- [19] Josep M. Guerrero, Juan C. Vasquez, José Matas, Luis García de Vicuña, and Miguel Castilla. Hierarchical control of droop-controlled ac and dc microgrids—a general approach toward standardization. *IEEE Transactions on Industrial Electronics*, 58(1):158–172, 2011.
- [20] M. Liserre R. Teodorescu and P. Rodriguez. *Grid Converters for Photovoltaic and Wind Power Systems*. A John Wiley and Sons, Ltd, 2011.
- [21] S Narendiran, Sarat Kumar Sahoo, Raja Das, and Ashwin Kumar Sahoo. Fuzzy logic controller based maximum power point tracking for pv system. In *2016 3rd International Conference on Electrical Energy Systems (ICEES)*, pages 29–34, 2016.

- [22] Youcef Soufi, Mohcene Bechouat, Sami Kahla, and Kais Bouallegue. Maximum power point tracking using fuzzy logic control for photovoltaic system. In *2014 International Conference on Renewable Energy Research and Application (ICR-ERA)*, pages 902–906, 2014.
- [23] Mohammad Iman Bahari, Pouya Tarassodi, Yousef Mazaheri Naeini, Ali Kalantari Khalilabad, and Paimaneh Shirazi. Modeling and simulation of hill climbing mppt algorithm for photovoltaic application. In *2016 International Symposium on Power Electronics, Electrical Drives, Automation and Motion (SPEEDAM)*, pages 1041–1044, 2016.
- [24] Davide Andrea. 2020.
- [25] Manuel Baumann, Jens Peters, Marcel Weil, Carolina Marcelino, Paulo Almeida, and Elizabeth Wanner. Environmental impacts of different battery technologies in renewable hybrid micro-grids. In *2017 IEEE PES Innovative Smart Grid Technologies Conference Europe (ISGT-Europe)*, pages 1–6, 2017.
- [26] R. Handa S. Shaw A. ter Shure B. Westlake, H. Kamath. Ensuring a clean grid—batteries not excluded. *EPRI Journal*, 2016.
- [27] Teke Gush, Chul-Hwan Kim, Samuel Admasie, Ji Kim, and JIN-SOL SONG. Optimal smart inverter control for pv and bess to improve pv hosting capacity of distribution networks using slime mould algorithm. *IEEE Access*, 9, 03 2021.
- [28] Sampath Jayalath and M. Hanif. An lcl-filter design with optimum total inductance and capacitance. *IEEE Transactions on Power Electronics*, PP:1–1, 09 2017.

- [29] Bohirjon Sharifov, Rustam Yunusov, Kamol Gulyamov, Sarfarozi Dovudov, Murodbek Safaraliev, and Anvari Ghulomzoda. The mathematical model of pulse width modulation frequency converter. In *2021 Ural-Siberian Smart Energy Conference (USSEC)*, pages 81–84, 2021.
- [30] A. Yazdani and R.Iravani. *Voltage-Sourced Converters in Power Systems*. A John Wiley and Sons, Ltd, 2010.
- [31] Amirnaser Yazdani. Control of an islanded distributed energy resource unit with load compensating feed-forward. In *2008 IEEE Power and Energy Society General Meeting - Conversion and Delivery of Electrical Energy in the 21st Century*, pages 1–7, 2008.
- [32] Oben Dag and Behrooz Mirafzal. On stability of islanded low-inertia microgrids. In *2016 Clemson University Power Systems Conference (PSC)*, pages 1–7, 2016.
- [33] P.Pourbeik. Wecc second generation wind turbine models. 01 2014.

APPENDIX A:
WECC DYNAMIC MODULES

In recent years, Energy Storage systems are being penetrated in many power utility companies. They are connected to transmission and distribution systems for a variety of reasons. Some of their uses are for power shaving and shedding, supporting grid frequency and voltage by optimizing the power quality. Also batteries can store energy for later use. WECC has proposed several ‘generic’ modules to model the system as shown in the following figure A.1

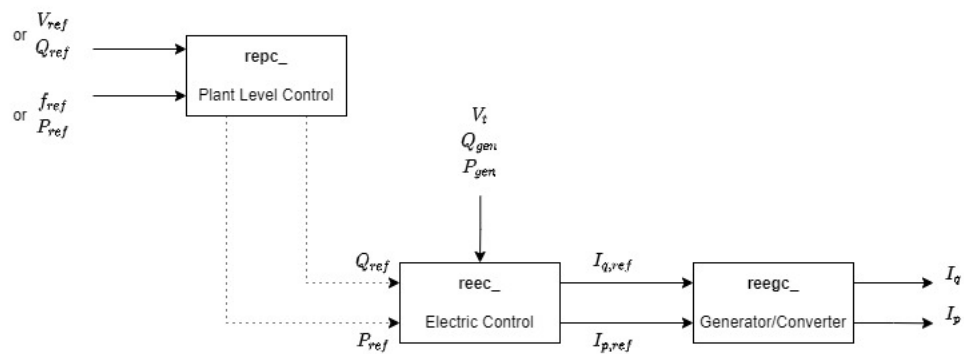


Figure A.1: Block Diagram Representation of the BESS Model

1- REGC_Module: This module is used to represent the interface between the converter with the grid. It takes the real and reactive power commands from the main electric control REEC_. It creates the real and reactive currents that are injected into the grid. The newest version REGC_b has improved numerical performance. A block diagram from [33] is shown in Figure A.2.

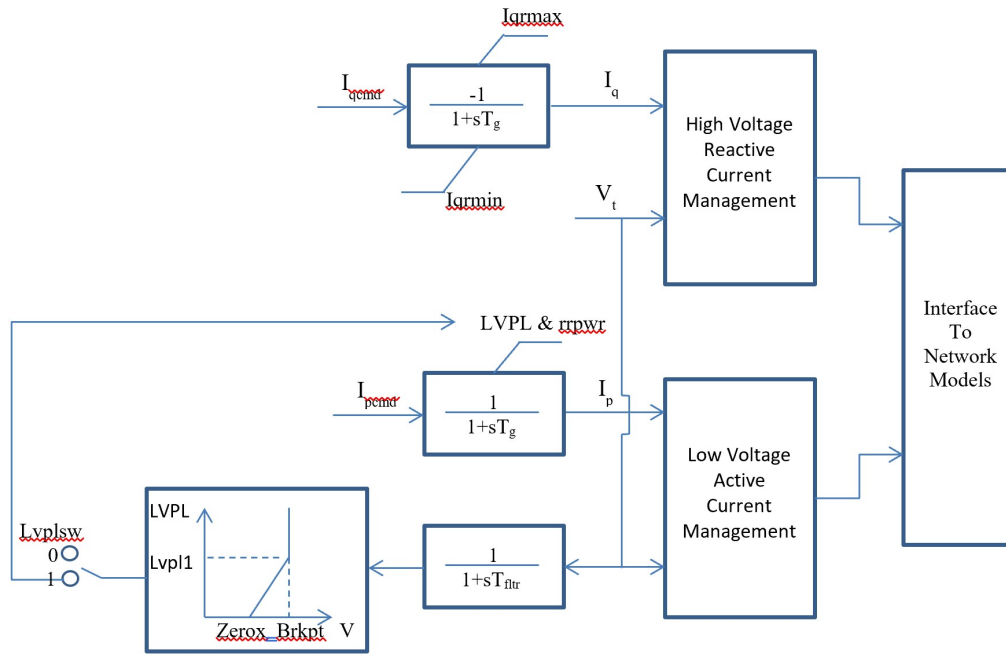


Figure A.2: Block Diagram of Renewable Energy Generator/Converter Module

2- REEC_Module: This module has multiple versions , one is for PV and wind turbine generators as REEC_A and another one is the REEC_C which is an augmented version from the previous one, and is more compatible with BESS. The most recent version is the REEC.D. This module provides real and reactive current commands to REGC_module. It allows for current compensation and the most recent version allows more points to be used to define current limits. The overall structure of the module is shown in [33] in Figure A.3.

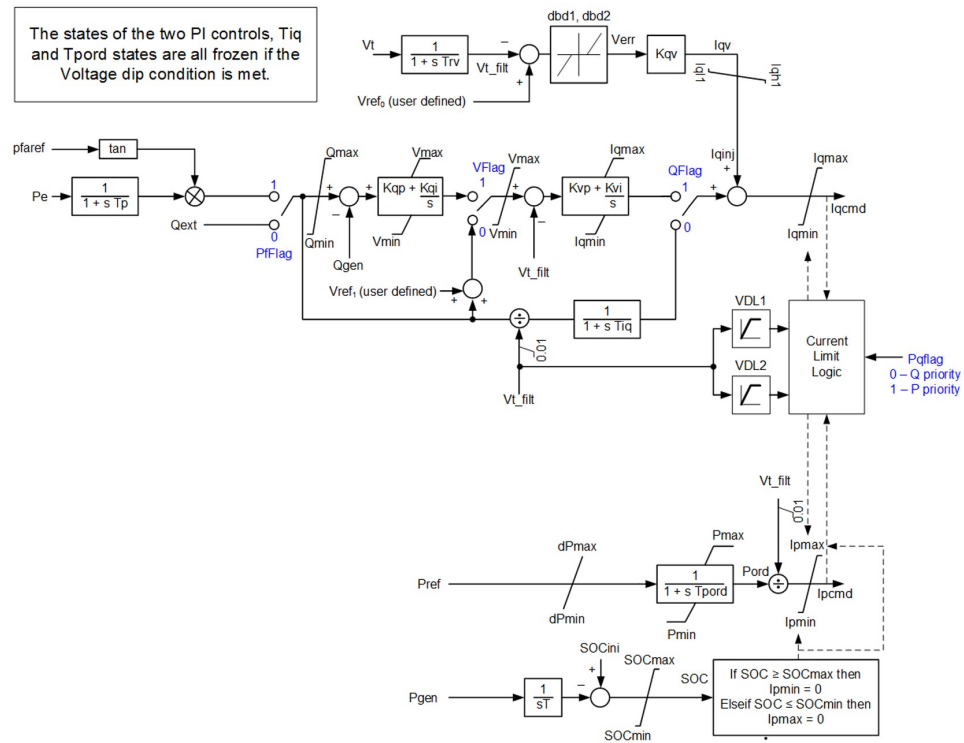


Figure A.3: Block Diagram of Renewable Energy Control Module

3- REPC_Module: Is used to represent the plant controller. The most recent version is REPC_C and includes Multi-state system (MSS) logic and allows power factor control. More information can be found in in [33] including a description for parameters and acronyms.

APPENDIX B:
PASSIVE ELEMENTS IN
DQ0-TRANSFORMATION

The dq0-transformation represents the sinusoidal AC components as constants in order to simplify the analysis of AC power systems. This transformation is considered more accurate than other approximations. In this Appendix, the modelling of linear passive components such as resistors, inductors and capacitors will be explained more explicitly.

Assume a symmetrical balanced three-phase resistor R is modeled as follows,

$$V_{abc} = R.I_{abc}, \quad (\text{B.1})$$

Which also can be represented as follows,

$$\begin{bmatrix} V_a \\ V_b \\ V_c \end{bmatrix} = R \begin{bmatrix} I_a \\ I_b \\ I_c \end{bmatrix} \quad (\text{B.2})$$

By multiplying both sides of the equation by Matrix (B.3),

$$A^{-1} = \frac{2}{3} \begin{bmatrix} \cos(\theta) & \cos(\theta - \frac{2\pi}{3}) & \cos(\theta + \frac{2\pi}{3}) \\ -\sin(\theta) & -\sin(\theta - \frac{2\pi}{3}) & -\sin(\theta + \frac{2\pi}{3}) \\ \frac{1}{2} & \frac{1}{2} & \frac{1}{2} \end{bmatrix} \quad (\text{B.3})$$

We get,

$$\begin{bmatrix} V_d \\ V_q \\ V_0 \end{bmatrix} = R \begin{bmatrix} I_d \\ I_q \\ I_0 \end{bmatrix} \quad (\text{B.4})$$

Matrix (B.4) is considered the dq0 model of a symmetrically balanced three-phase resistor.

The modelling of an inductor in the dq0-frame is considered more complicated. Assume a symmetrically three-phase inductor L, which is modelled as follows,

$$\begin{bmatrix} V_a \\ V_b \\ V_c \end{bmatrix} = L \frac{d}{dt} \begin{bmatrix} I_a \\ I_b \\ I_c \end{bmatrix} \quad (\text{B.5})$$

And using the identity which states $[i_a, i_b, i_c]^T = A[i_d, i_q, i_0]^T$, where A is Matrix (3.3) yields to,

$$\begin{bmatrix} V_a \\ V_b \\ V_c \end{bmatrix} = L \frac{d}{dt} \cdot A \begin{bmatrix} I_d \\ I_q \\ I_0 \end{bmatrix} \quad (\text{B.6})$$

By applying the derivative product rule leads to,

$$\begin{bmatrix} V_a \\ V_b \\ V_c \end{bmatrix} = L \frac{d}{dt} \cdot A \begin{bmatrix} I_d \\ I_q \\ I_0 \end{bmatrix} + L \cdot A \frac{d}{dt} \begin{bmatrix} I_d \\ I_q \\ I_0 \end{bmatrix} \quad (\text{B.7})$$

Using direct computation we can conclude that,

$$\frac{d}{dt} \cdot A = A \cdot \omega \quad (\text{B.8})$$

Where ω is,

$$\omega = \begin{bmatrix} 0 & \frac{d\theta}{dt} & 0 \\ -\frac{d\theta}{dt} & 0 & 0 \\ 0 & 0 & 0 \end{bmatrix} \quad (\text{B.9})$$

And now if we substitute Matrix (B.8) and (B.9) in (B.7), we get,

$$\begin{bmatrix} V_a \\ V_b \\ V_c \end{bmatrix} = L.A.\omega \begin{bmatrix} I_d \\ I_q \\ I_0 \end{bmatrix} + L.A.\frac{d}{dt} \begin{bmatrix} I_d \\ I_q \\ I_0 \end{bmatrix} \quad (\text{B.10})$$

and by multiplying both sides of the equation by A^{-1} , we get,

$$\begin{bmatrix} V_d \\ V_q \\ V_0 \end{bmatrix} = -L.\omega \begin{bmatrix} I_d \\ I_q \\ I_0 \end{bmatrix} + L.\frac{d}{dt} \begin{bmatrix} I_d \\ I_q \\ I_0 \end{bmatrix} \quad (\text{B.11})$$

Which is exactly the same as,

$$\frac{d}{dt} \begin{bmatrix} I_d \\ I_q \\ I_0 \end{bmatrix} = \omega \begin{bmatrix} I_d \\ I_q \\ I_0 \end{bmatrix} + \frac{1}{L} \begin{bmatrix} V_d \\ V_q \\ V_0 \end{bmatrix} \quad (\text{B.12})$$

Same thing applies to a capacitive symmetrical configuration,

$$\frac{d}{dt} \begin{bmatrix} V_d \\ V_q \\ V_0 \end{bmatrix} = \omega \begin{bmatrix} V_d \\ V_q \\ V_0 \end{bmatrix} + \frac{1}{C} \begin{bmatrix} I_d \\ I_q \\ I_0 \end{bmatrix} \quad (\text{B.13})$$